Atmos. Chem. Phys., 16, 1139–1160, 2016
www.atmos-chem-phys.net/16/1139/2016/
doi:10.5194/acp-16-1139-2016

Atmospheric Chemistry and Physics
Open Access
EGU

Wintertime aerosol chemical composition, volatility, and spatial variability in the greater London area

L. Xu[1], L. R. Williams[2], D. E. Young[3,a], J. D. Allan[3,4], H. Coe[3], P. Massoli[2], E. Fortner[2], P. Chhabra[2,b], S. Herndon[2], W. A. Brooks[2], J. T. Jayne[2], D. R. Worsnop[2], A. C. Aiken[5], S. Liu[5,c], K. Gorkowski[5,d], M. K. Dubey[5], Z. L. Fleming[6,7], S. Visser[8], A. S. H. Prévôt[8], and N. L. Ng[1,9]

[1]School of Chemical and Biomolecular Engineering, Georgia Institute of Technology, Atlanta, GA, USA
[2]Aerodyne Research Inc., Billerica, MA, USA
[3]School of Earth, Atmospheric and Environmental Sciences, University of Manchester, Manchester, UK
[4]National Centre for Atmospheric Science, University of Manchester, Manchester, UK
[5]Earth and Environmental Sciences Division, Los Alamos National Laboratory, Los Alamos, NM, USA
[6]Department of Chemistry, University of Leicester, Leicester, UK
[7]National Centre for Atmospheric Science, University of Leicester, Leicester, UK
[8]Laboratory of Atmospheric Chemistry, Paul Scherrer Institute, Villigen, Switzerland
[9]School of Earth and Atmospheric Sciences, Georgia Institute of Technology, Atlanta, GA, USA
[a]now at: Department of Environmental Toxicology, University of California, Davis, CA, USA
[b]now at: PerkinElmer Inc., Hopkinton, MA, USA
[c]now at: Cooperative Institute for Research in the Environmental Sciences, University of Colorado, Boulder, CO, USA
[d]now at: Center for Atmospheric Particle Studies, Carnegie Mellon University, Pittsburgh, PA, USA

Correspondence to: N. L. Ng (ng@chbe.gatech.edu)

Received: 13 July 2015 – Published in Atmos. Chem. Phys. Discuss.: 28 August 2015
Revised: 10 December 2015 – Accepted: 13 January 2016 – Published: 2 February 2016

Abstract. The composition of PM_1 (particulate matter with diameter less than 1 µm) in the greater London area was characterized during the Clean Air for London (ClearfLo) project in winter 2012. Two high-resolution time-of-flight aerosol mass spectrometers (HR-ToF-AMS) were deployed at a rural site (Detling, Kent) and an urban site (North Kensington, London). The simultaneous and high-temporal resolution measurements at the two sites provide a unique opportunity to investigate the spatial distribution of PM_1. We find that the organic aerosol (OA) concentration is comparable between the rural and urban sites, but the contribution from different sources is distinctly different between the two sites. The concentration of solid fuel OA at the urban site is about twice as high as at the rural site, due to elevated domestic heating in the urban area. While the concentrations of oxygenated OA (OOA) are well-correlated between the two sites, the OOA concentration at the rural site is almost twice that of the urban site. At the rural site, more than 70 % of the carbon in OOA is estimated to be non-fossil, which suggests that OOA is likely related to aged biomass burning considering the small amount of biogenic SOA in winter. Thus, it is possible that the biomass burning OA contributes a larger fraction of ambient OA in wintertime than what previous field studies have suggested.

A suite of instruments was deployed downstream of a thermal denuder (TD) to investigate the volatility of PM_1 species at the rural Detling site. After heating at 250 °C in the TD, 40 % of the residual mass is OA, indicating the presence of non-volatile organics in the aerosol. Although the OA associated with refractory black carbon (rBC; measured by a soot-particle aerosol mass spectrometer) only accounts for < 10 % of the total OA (measured by a HR-ToF-AMS) at 250 °C, the two measurements are well-correlated, suggesting that the non-volatile organics have similar sources or have undergone similar chemical processing as rBC in the atmosphere. Although the atomic O : C ratio of OOA is substantially larger than that of solid fuel OA and hydrocarbon-like OA, these three factors have similar volatility, which is inferred from

the change in mass concentration after heating at 120 °C. Finally, we discuss the relationship between the mass fraction remaining (MFR) of OA after heating in the TD and atomic O : C of OA and find that particles with a wide range of O : C could have similar MFR after heating. This analysis emphasizes the importance of understanding the distribution of volatility and O : C in bulk OA.

1 Introduction

Particulate matter (PM) concentration in the greater London area often exceeds European air quality limits, causing adverse effects on the health of habitants in this area (Harrison et al., 2012; Bohnenstengel et al., 2014). Therefore, it is critical to identify the PM sources in order to implement effective strategies to control ambient pollutants. The Clean Air for London (ClearfLo) project aimed to study boundary layer pollution in the greater London area through comprehensive measurements of meteorology, gaseous, and particulate composition (Bohnenstengel et al., 2014). Multiple monitoring sites were set up in both urban and rural areas around London to quantify the urban increment in gas-phase and particle-phase pollutants.

Previous studies in the greater London area have repeatedly shown that the concentration of elemental carbon (EC) is higher in urban sites than rural sites due to elevated levels of primary emissions such as vehicle exhaust and wood smoke (Crilley et al., 2015; Yin et al., 2015). The origin of organic carbon (OC) at urban and rural sites is instead more challenging to elucidate considering the myriad of different OC sources. Based on the ratios among multiple tracers (e.g., EC / OC and levoglucosan / OC) from different sources, Crilley et al. (2015) estimated that the concentration of primary OC from vehicle emissions was higher in an urban area compared to a rural area in the UK. Many studies have applied the chemical mass balance (CMB) model for OC apportionment (Yin et al., 2010; Crilley et al., 2015; Yin et al., 2015). However, due to the uncertainties in the source profiles and the number of organic tracers included in the model, the concentration of secondary OC is highly uncertain. In addition, OC measurements based on filter samples on a daily basis limit the temporal resolution of rural vs. urban comparisons.

Factor analysis via positive matrix factorization (PMF) of aerosol mass spectrometer (AMS) measurements is another widely used method to identify sources of organic aerosol (OA) (Jimenez et al., 2009; Lanz et al., 2007; Ng et al., 2010; Xu et al., 2015a). Based on factor analysis of AMS measurements around the world, Zhang et al. (2007) observed that the contribution of hydrocarbon-like OA (a surrogate for primary OA) to total OA decreased from urban sites to rural sites, but the oxygenated OA (a surrogate for secondary OA), showed the opposite trend. The authors also showed that the average OA concentration is substantially lower in rural sites than urban sites (2.8 vs. 7.6 $\mu g\,m^{-3}$). However, the trend observed in Zhang et al. (2007) needs to be further verified since the urban vs. rural comparisons are not based on simultaneous measurements between paired locations.

Comparison based on simultaneous measurements between different sites, especially between rural and urban sites, is useful to identify regional and local sources of OA. For example, by comparing concurrent AMS measurements of OA at multiple sites in the greater Atlanta area, USA, Xu et al. (2015a, b) showed that the OA was spatially homogeneous and mainly regional in summer, but the OA showed substantial spatial variability in winter. Based on PMF analysis of AMS measurements, Crippa et al. (2013) investigated the correlation of various OA subtypes between three urban sites located in a 20 km radius region in Paris, France, during winter 2010. The authors observed that the secondary OA factors had substantially better correlation between different sites than the primary OA factors, including OA from vehicles, biomass burning, and cooking. However, a rural vs. urban comparison was not performed in Crippa et al. (2013).

In addition to OA sources, the volatility of OA is an important property since it directly determines the gas–particle partitioning. The thermal denuder (TD) has been used widely to measure the aerosol volatility (An et al., 2007; Huffman et al., 2008; Saleh et al., 2012). Many previous studies inferred the volatility from the mass fraction remaining (MFR) or volume fraction remaining (VFR), which is calculated as the ratio of the species mass (or volume) concentration after heating to an elevated temperature in the TD to the species mass (or volume) concentration without heating (An et al., 2007; Huffman et al., 2009b; Jonsson et al., 2007; Lee et al., 2011; Stanier et al., 2007; Grieshop et al., 2009b; Xu et al., 2014; Huffman et al., 2009a). Larger MFR is used as an indication of lower volatility of aerosol. However, Saleh et al. (2011) suggested that it is misleading to use MFR as an indication of volatility. This is mainly because the MFR is an extensive parameter (which explicitly depends on the initial mass concentration) while aerosol volatility is an intensive property (which depends only on chemical nature of the compounds in a mixture). Instead of MFR, Saleh et al. (2011) presented that the change in mass concentration when reaching equilibrium upon heating (i.e., ΔC) is an appropriate measure of volatility.

Although multiple previous studies have investigated the volatility of laboratory-generated OA (An et al., 2007; Huffman et al., 2009b; Jonsson et al., 2007; Lee et al., 2011; Stanier et al., 2007; Grieshop et al., 2009b; Xu et al., 2014), there are only limited studies on the volatility of ambient OA, especially on the volatility of OA from different sources (Hildebrandt et al., 2010; Huffman et al., 2009a; Massoli et al., 2015; Paciga et al., 2015). Previous studies have shown the presence of non-volatile organics in ambient aerosol even after heating to high temperatures (i.e., 230–300 °C) (Huffman et al., 2009a; Häkkinen et al., 2012; Poulain et al., 2014; Massoli et al., 2015; Liu et al., 2015). However, the sources

of non-volatile organics are uncertain. Häkkinen et al. (2012) and Poulain et al. (2014) found that the non-volatile residuals correlated with anthropogenic tracers, such as BC and polycyclic aromatic hydrocarbons (PAHs), implying that the non-volatile species are possibly linked to anthropogenic emissions. However, in both studies, the TD was only applied upstream of a scanning mobility particle sizer (SMPS); therefore, the composition of remaining compounds was not directly measured but only conjectured. Massoli et al. (2015) coupled a TD with a soot-particle AMS (SP-AMS) during measurements in California. The authors observed the existence of refractory OA (i.e., detectable via laser vaporization in the SP-AMS, but not detectable by vaporization at 600 °C in the standard AMS), which was present in the fresh urban air masses, but not in the aged air masses.

Many studies have used the degree of oxidation of OA, such as atomic O : C ratio and oxidation state (OS) as a proxy for volatility. For example, two oxygenated OA factors with high but different O : C ratio are often resolved from PMF analysis on AMS data. These two oxygenated OA factors are often named semi-volatile OOA (SVOOA) and low-volatility OOA (LVOOA) based on the volatility inferred from O : C values (Ng et al., 2010; Huang et al., 2010; Mohr et al., 2012; Jimenez et al., 2009). In a laboratory study on toluene SOA, Hildebrandt Ruiz et al. (2015) observed a linear relationship between OS and effective saturation concentration of the aerosol. However, for both ambient measurements and laboratory studies, it is uncertain whether the O : C or OS of bulk OA is a good indicator of volatility. In Mexico City and Riverside, CA, Huffman et al. (2009a) showed that the O : C ratio of the thermally denuded OA increased with TD heating temperature, which suggests that the O : C is inversely correlated with the volatility of organic aerosol (i.e., the residual OA with lower volatility after heating has a higher O : C). In contrast, only a weak correlation between O : C and volatility was observed in Hildebrandt et al. (2010), who measured the volatility of ambient OA in Finokalia, Greece. The authors found that between thermally denuded OA and ambient OA, the mass spectrum was similar and the difference in f_{44} (i.e., fraction of organic signal at m/z 44, which has a linear correlation with O : C) was not statistically significant. This indicates that the degree of oxidation does not change after evaporation of relatively volatile species. In addition, various relationships between O : C and volatility (inferred from the MFR) have been observed in previous laboratory studies on different SOA systems (Grieshop et al., 2009b; Qi et al., 2010; Donahue et al., 2012; Kroll et al., 2009; Tritscher et al., 2011; Xu et al., 2014). For example, Xu et al. (2014) observed that while the O : C of isoprene SOA formed in the laboratory without additional NO remained fairly constant ($\sim$ 0.6) during photochemical aging, the VFR increased over time. Grieshop et al. (2009b) showed that during photochemical aging, OA from wood fires became more oxidized (i.e., O : C increases), but the MFR remained constant. Donahue et al. (2012) studied the photochemical aging of α-pinene ozonolysis SOA and observed that while the OA became more oxidized (i.e., O : C increases), the VFR decreased with aging. The authors proposed that the photochemical aging produced both relatively volatile products and more oxidized products, which broadened the volatility distribution of the OA (Donahue et al., 2012). In summary, while SOA becomes progressively more oxidized (i.e., O : C increases) during aging, the MFR or VFR exhibits different trends (i.e., increases, stays constant, or decreases over time) for different SOA systems.

Figure 1. Geographical locations of the sampling sites (i.e., North Kensington and Detling) in this study. The region circled by the M25 motorway is the greater London area. The map is adapted from Google Maps.

In this study, we performed simultaneous measurements at a rural site (Detling, Kent) and an urban site (North Kensington, London) in the greater London area in winter 2012 using two Aerodyne high-resolution time-of-flight mass spectrometers (HR-ToF-AMS) (DeCarlo et al., 2006). The comparison of the simultaneous, high-temporal resolution measurements and the OA source apportionment by PMF analysis provide insights into sources of wintertime OA in the greater London area. Since biogenic emissions are low in winter, these measurements allow for a more direct evaluation of the contributions of anthropogenic emissions to OA formation. We also deployed a thermal denuder upstream of a suite of instruments to directly characterize the non-volatile residual at 250 °C. Furthermore, we investigated the volatility of different OA sources and systematically evaluated the relationship between O : C and OA volatility.

2 Method

2.1 Sampling sites and meteorological conditions

Measurements were performed as part of the ClearfLo project. An overview of the ClearfLo field campaign can be found in Bohnenstengel et al. (2014). The main goal of the ClearfLo project was to study boundary layer pollution in the greater London area by comprehensive measurements of

meteorology, gaseous composition, and particulate composition. Multiple monitoring sites were set up in both urban and rural areas and at different elevations (street and elevated level) to perform year-long measurements across London. In addition, two intensive observation periods (IOPs) were conducted during winter (January–February, 2012) and summer (July–August, 2012). Data presented in this paper were collected at the Detling site and the North Kensington (NK) site during the winter IOP. Figure 1 shows the locations of both sites. The NK site (51.521055° N, 0.213432° W) is an urban background site located in a residential area, 7 km to the west of central London. The Detling site (51.301931° N, 0.589494° E) is a rural site located on a plateau (200 m a.s.l.), 45 km southeast of London. The closest road is about 150 m (south), which carries ∼ 42 000 vehicles per day (www.dft.gov.uk/traffic-counts). The typical meteorological data (temperature, relative humidity, and wind speed) at the Detling site are shown in Fig. S1a in the Supplement. The campaign-averaged temperature was 6 °C. In the diurnal variation, the highest temperature was ∼ 8 °C at 14:00 (local time) and the lowest temperature was ∼ 5 °C at 07:00. The relative humidity was 83 % on average. The wind speed was 5.8 m s^{-1} on average, but it occasionally reached 10 m s^{-1}. The wind rose plot is shown in Fig. S1b. The prevailing wind was from the northeast and the southwest.

2.2 Instrumentation

In the following discussions on instrumental setup and data analysis methods, we will focus on the rural Detling site. For instruments deployed at the urban NK site, only the HR-ToF-AMS ambient measurements are included in this study. The data analysis of HR-ToF-AMS at the urban site is similar to that at the rural site, which will be discussed below. Details regarding the measurements at the NK site can be found in Young et al. (2015a).

A suite of instruments was deployed at the Detling site to characterize both the gas-phase and particle-phase composition. Instruments of interest to this study are shown in Fig. S2 and are described below. Ambient particles were sampled through a $PM_{2.5}$ cyclone and then directed through either a thermal denuder line (denoted as TD line) or a bypass line before being analyzed by downstream instruments. The TD (Aerodyne), designed based on Huffman et al. (2008), consists of a 22″ long stainless steel tube operated at elevated temperatures (i.e., heated section), followed by a 24″ section of activated charcoal held at room temperature to adsorb the evaporated components from particles. The heating section was operated at 120 and 250 °C. The aerosol residence time in the heating section of the TD was 5.3 s at the experimental flow rate (2.3 L min^{-1} determined by the sampling rate of instruments downstream of the TD). Caution is required when comparing the results between different studies with a TD because the TD configuration and residence times can be different. Particle loss in the TD was characterized based on the single particle soot photometer (SP2) refractory black carbon (rBC) mass measurement during the field campaign, since rBC does not evaporate even at 250 °C. The transmission efficiency of TD is about 90 % (Fig. S3), similar to the values reported in previous studies with similar TD configurations (Huffman et al., 2008; Massoli et al., 2015). The timescale to reach thermodynamic equilibrium in a given TD depends on a number of factors, such as TD temperature, aerosol mass concentration, aerosol diameter, and mass accommodation coefficient (Riipinen et al., 2010; An et al., 2007; Saleh et al., 2011). In this study, we calculate the characteristic time for aerosol equilibration by following the algorithm in Saleh et al. (2011). To evaluate the equilibration timescale in the TD, the authors started with the mass transfer equation (Eq. 1) and then obtained the characteristic time for aerosol equilibration (τ in Eq. 2) by performing dimensional analysis.

$$\frac{dC_a}{dt} = -2\pi d_p D F N_{tot}(K C_{g,sat} - C_g) \quad (1)$$

$$\tau = \frac{1}{2\pi d_p D F N_{tot}} \quad (2)$$

$$F = \frac{1 + Kn}{1 + 0.3773Kn + 1.33Kn(1 + Kn)/\partial} \quad (3)$$

In the equations, C_a, C_g, and $C_{g,sat}$ are the aerosol-phase concentration, gas-phase concentration, and gas-phase saturation concentration, respectively. N_{tot} is the total number concentration, d_p is the particle size, D is the diffusion coefficient in the gas phase, K is the Kelvin effect correction, and F is the Fuchs–Sutugin correction, which is calculated by Eq. (3). In Eq. (3), Kn is the Knudsen number and α is the accommodation coefficient. D is on the order of 10^{-5} m^2 s^{-1} according to Tang et al. (2015) and α is on the order of 0.1 as shown in Saleh et al. (2012). By using the campaign-averaged particle number concentration (i.e., 4.28×10^3 cm^{-3}) and the mode of the particle number distribution (i.e., 87 nm) in our study, we estimate that the characteristic equilibration time is about 1600 s, which is orders of magnitude longer than that residence time (5 s) in the TD. Since the evaporation process is likely far away from equilibrium, the gas-phase saturation ratio is small and the particles are likely evaporating in a vapor-free environment. Under this assumption, the gas-phase vapor concentration (i.e., C_g) in the mass transfer equation (Eq. 1) can be neglected. After integration over the residence time in the TD, the change in mass concentration upon heating (ΔC_a) can be calculated by Eq. (4), in which $t_{residence}$ is the residence time in TD and the $\overline{C^*}$ is the evaporation-time-averaged saturation concentration. Thus, the ΔC_a for each component is proportional to its $\overline{C^*}$ because the other parameters are the same assuming the compounds are internally mixed.

$$\Delta C_{\mathrm{a}} = C_{t=0} - C_{t_{\mathrm{residence}}} = \int_0^{t_{\mathrm{residence}}} \frac{K C_{\mathrm{g,sat}}}{\tau} \mathrm{d}t = \frac{t_{\mathrm{residence}}}{\tau} K \overline{C^*} \quad (4)$$

A HR-ToF-AMS (Aerodyne), a SP-AMS (Aerodyne), a SP2 (DMT), and a SMPS (TSI) were placed downstream of the TD. These four instruments alternated between sampling the bypass line (i.e., ambient) and the TD line (i.e., thermally denuded) every 10 min. When the instruments were sampling through the bypass line, the heating section of TD was adjusted to the subsequent temperature set point. The MFR was determined by comparing the measurements between bypass line and TD line.

The HR-ToF-AMS provides real-time measurements of the chemical composition and size distribution of submicron non-refractory species (NR-PM_1) and has been described in detail previously (Canagaratna et al., 2007; DeCarlo et al., 2006). In brief, the HR-ToF-AMS samples particles through an aerodynamic lens and then impacts the focused particle beam on a heated tungsten surface ($\sim 600\,^{\circ}\mathrm{C}$). The resultant vapors are ionized by electron impact ionization and the ions are analyzed using time-of-flight mass spectrometry. We used the ambient gas-phase CO_2 concentration (measured by a LI-COR CO_2 gas analyzer with 1 min resolution) to correct for the gas-phase interference in the particle-phase CO_2^+ signals for both the bypass line and TD line. The assumption behind this correction for the TD line is that the CO_2 generated in the TD, if it exists, is negligible. Unless otherwise specified, the elemental ratios, such as atomic O : C and H : C, were calculated based on the latest recommendation by Canagaratna et al. (2015), who modified the original method developed for the HR-ToF-AMS (Aiken et al., 2007, 2008). The HR-ToF-AMS data were analyzed using the standard AMS analysis toolkits SQUIRREL v1.56A and PIKA v1.15.

The SP-AMS measures the chemical composition of rBC-containing particles by using an intracavity laser vaporizer (1064 nm). The detailed working principles of SP-AMS are extensively discussed in Onasch et al. (2012). In brief, after being focused through an aerodynamic lens, the rBC-containing particles are heated and vaporized by laser absorption. The chemical composition of both the rBC and any associated coatings are analyzed via high-resolution mass spectrometry. The SP-AMS data presented in this paper were obtained between 5 and 15 February, 2012, when the instrument was operated in the laser vaporizer-only configuration; that is, only rBC-associated species were detected. Analysis and interpretation of the SP-AMS measurements for the entire deployment at Detling are presented in Williams et al. (2016).

The SP2 measures rBC using laser-induced incandescence. The method has been described previously (Schwarz et al., 2006; Stephens et al., 2003). In brief, a 1064 nm Nd:YAG laser irradiates the particles as they enter the SP2, where upon vaporization and incandescence is induced in the particles containing rBC. The incandescence signal is proportional to the mass of rBC per particle, and with the sampling volume, rBC mass concentrations are quantified. The SP2 at the Detling site was calibrated using fullerene soot (Alfa Aesar, Inc., Ward Hill, Massachusetts; Stock no. 40971, Lot no. L18U002). Fullerene soot is an rBC surrogate used for calibration of the SP2 due to its known density and similarities to ambient rBC (Baumgardner et al., 2012; Laborde et al., 2012). Data analysis was performed with the Paul Scherrer Institute Toolkit (PSI; Martin Gysel) developed for SP2 analysis within Igor Pro (Wavemetrics, Inc.).

2.3 Collection efficiency of the HR-ToF-AMS

In order to provide quantitative data from HR-ToF-AMS measurements, the particle collection efficiency (CE), which is largely due to particles bouncing on the vaporizer, needs to be evaluated. For the bypass line, we calculated the CE based on the composition-dependent algorithm proposed by Middlebrook et al. (2012) (i.e., CDCE). The CDCE for the bypass line ranges from 0.45 to 0.97, with the campaign-averaged value 0.52 ± 0.08 (1 standard deviation). In order to validate the application of CDCE, we converted the mass concentrations of ambient non-refractory species measured by HR-ToF-AMS (after CDCE correction) together with the mass concentration of refractory species (i.e., rBC and crustal material) to volume using Eq. (5) and then compared the calculated volume with SMPS measurements.

$$\mathrm{volume} = \frac{[NO_3^-] + [SO_4^{2-}] + [NH_4^+]}{1.75} + \frac{[Cl^-]}{1.52} + \frac{[\mathrm{org}]}{\rho_{\mathrm{org}}} + \frac{[\mathrm{crustal\ material}]}{2.7} + \frac{[\mathrm{BC}]}{0.73} \quad (5)$$

In Eq. (5), $1.75\,\mathrm{g\,cm^{-3}}$ was used as the density for inorganic nitrate, sulfate, and ammonium, and $1.52\,\mathrm{g\,cm^{-3}}$ was used as the density for chloride (Poulain et al., 2014). The density of ambient organics was estimated using atomic O : C and H : C ratios as suggested by Kuwata et al. (2012). It is noted that the O : C and H : C ratios calculated based on Aiken et al. (2008) were used in the density estimation in order to be consistent with Kuwata et al. (2012). The organic density was estimated to be 1.30, 1.42, and $1.68\,\mathrm{g\,cm^{-3}}$ for bypass line, TD = 120 °C, and TD = 250 °C, respectively. The estimated density values were within the literature range (Hallquist et al., 2009). The concentration of crustal material was estimated by summing the normal oxides (Na_2O, MgO, Al_2O_3, SiO_2, CaO, K_2O, FeO, Fe_2O_3, and TiO_2) of tracer elements (Malm et al., 1994). The tracer elements were measured by $PM_{1.0–0.3}$ rotating drum impactors and analyzed by synchrotron radiation-induced X-ray fluorescence spectrometry (Visser et al., 2015). The density of crustal material

($2.7\,\mathrm{g\,cm^{-3}}$) was adapted from Lide (1991). The rBC concentration was measured by the SP2. For the rBC density, many previous studies have used $1.77\,\mathrm{g\,cm^{-3}}$ (Salcedo et al., 2006; Poulain et al., 2014; Huffman et al., 2009a). However, we note that $1.77\,\mathrm{g\,cm^{-3}}$ (adapted from Park et al., 2004) is the inherent material density of diesel soot particles. If the inherent material density is used, one needs to consider the non-sphericity of rBC when comparing the calculated volume to the SMPS volume as the particles are assumed to be spherical when estimating the SMPS volume. In order to circumvent this issue, we used an effective density of rBC in this study. Park et al. (2003) measured the effective density of diesel soot particles in the 50–300 nm range (mobility diameter) by using a Differential Mobility Analyzer – Aerosol Particle Mass (DMA-APM) analyzer system. The soot particles were firstly classified based on mobility diameter in DMA and the mass of classified particles was then measured by APM. The effective density was calculated with the following equation by assuming spherical particles:

$$\rho_{\mathrm{eff}} = \frac{\mathrm{mass}}{\frac{\pi}{6} d_{\mathrm{me}}^3}, \tag{6}$$

where d_{me} is the mobility equivalent diameter. Thus, applying the effective density measured by a DMA-APM system allows one to convert BC mass to its apparent volume, which is comparable to the SMPS volume. One factor that complicates the choice of rBC effective density is that this value decreases with increasing mobility diameter as shown in Park et al. (2003). Limited by the lack of knowledge of the size distribution (mobility diameter based) of rBC in our data, we calculated the average effective density based on all the values reported in Park et al. (2003) and used this average value ($0.73\,\mathrm{g\,cm^{-3}}$) in our study. This simplification is reasonable considering the following reasons. First, Crilley et al. (2015) estimated that 70 % of rBC at the Detling site is from traffic, which is similar to the BC types in Park et al. (2003). Second, the size distribution of total particles measured by SMPS in our study largely overlapped the size range studied in Park et al. (2003).

The calculated volume (based on HR-ToF-AMS + rBC + crustal material) was then compared with co-located SMPS measurements (Fig. 2). The SMPS measured the particle number distribution between 15.1 and 532.8 nm mobility diameter. The number distribution can be converted to a volume distribution assuming spherical particles. On average, the difference between the calculated volume and the SMPS volume was within 6 %, which validates the application of CDCE for the bypass line (Fig. 2a).

However, the CDCE is not applicable for the TD line because the CDCE algorithm is parameterized based on aerosol neutralization (Eq. 7), which depends strongly on the accuracy of the ammonium concentration measurement. The ammonium concentration decreased quickly upon heating and was close to the instrument detection limit at 250 °C. Thus, we evaluated the CE for the TD line by comparing the calculated volume (based on HR-ToF-AMS + rBC + crustal material) and the SMPS volume (Salcedo et al., 2006).

$$\begin{aligned}\text{neutralization} &= \frac{\mathrm{NH_{4,meas}}}{\mathrm{NH_{4,predict}}} \\ &= \frac{\mathrm{NH_{4,meas}}}{18 \times \left(\frac{\mathrm{SO_4}\times 2}{96} + \frac{\mathrm{NO_3}}{62} + \frac{\mathrm{Chl}}{35.5}\right)}\end{aligned} \tag{7}$$

We noted that the selection of the rBC density has a substantial effect on the TD line CE. For example, varying the rBC density from 1.77 to $0.60\,\mathrm{g\,cm^{-3}}$ (i.e., from the inherent material density to the effective density of 100 nm diesel soot particle reported in Park et al., 2003) changed the CE at 250 °C by a factor of 2 (Table S1). This sensitivity analysis highlighted the importance of the rBC density in applying this method to evaluate CE, especially for the TD line where rBC accounted for a large fraction of the mass concentration. In this study, since the TD line CE calculated with an rBC effective density of $0.73\,\mathrm{g\,cm^{-3}}$ (i.e., average value from Park et al., 2003) was close to the default value for CE (i.e., 0.45), we used 0.45 as the TD line CE in our analysis. As shown in Fig. 2b and c, the default CE results in a reasonable agreement between the calculated volume and the SMPS volume for the TD line. Specifically, the differences between the calculated volume and the SMPS volume are 14 and 11 % at 120 and 250 °C, respectively, which are within the range of measurement uncertainties. Future studies are warranted to comprehensively investigate the change of AMS CE after heating of the aerosol.

2.4 Data analysis

2.4.1 Positive matrix factorization analysis

PMF analysis has been widely used for aerosol source apportionment in the AMS community. This technique represents the observed data as a linear combination of factors with constant mass spectra but varying concentrations across time in the data set (Paatero and Tapper, 1994; Paatero, 1997). Two solvers have been used for PMF analysis of AMS data, PMF2 and the multilinear engine (ME-2). The PMF2 solver does not require a priori information, which avoids some subjectivity. The ME-2 solver uses a priori information to reduce rotational ambiguity among possible solutions (Canonaco et al., 2013; Paatero, 1999).

For the ambient OA measurements, we used the standard PMF2 solver, which does not include any a priori information. This analysis is denoted as $\mathrm{PMF_{ambient}}$ and was performed using the PMF Evaluation Toolkit (PET) software developed by Ulbrich et al. (2009). The error matrix was pre-treated based on the procedure in Ulbrich et al. (2009). m/z's with a signal-to-noise ratio in the range of 0.2–2 were down weighted by a factor of 2, and m/z's with a signal-to-noise ratio smaller than 0.2 were removed. Also, the con-

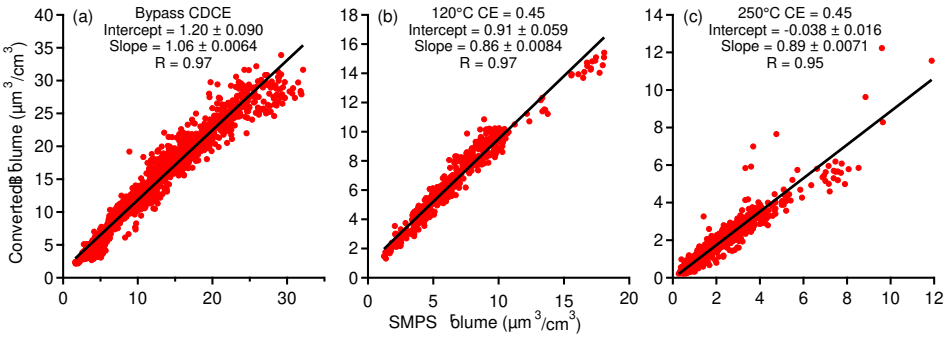

Figure 2. Scatter plot of converted volume (based on HR-ToF-AMS total + BC + crustal material) vs. the apparent volume estimated from SMPS measurement for **(a)** the bypass line and the TD line at **(b)** 120 °C and **(c)** 250 °C. The composition-dependent CE is applied to the bypass line HR-ToF-AMS measurements and CE = 0.45 is applied to the TD line HR-ToF-AMS measurements. The slopes and intercepts are obtained by orthogonal distance regression (ODR). The Pearson's R is obtained by linear least-squares fit.

tributions of O^+, HO^+, H_2O^+, CO^+, and CO_2^+ were down weighted to avoid excessive weighting of CO_2^+ and related fragments. Following the detailed procedure listed in Zhang et al. (2011), the PMF solutions were evaluated by investigating the key diagnostic plots (Fig. S4), mass spectral signatures, correlations with external tracers, and the diurnal profiles. The rotational ambiguity of the optimal solution was examined by changing the fpeak parameter from −1 to 1. In our case, an fpeak value of 0 ($Q/Q_{exp} = 1.804$) was selected because the correlations between factors and external tracers were not improved for fpeak values that were different from 0. We resolved three factors from $PMF_{ambient}$, i.e., hydrocarbon-like OA (HOA), solid fuel OA (SFOA), and oxygenated OA (OOA), which are discussed in Sect. 3.1. The choice of a three-factor solution is discussed in detail in the Supplement (Fig. S5).

For the TD line measurements, we first tried the PMF2 solver on the combined ambient and thermally denuded OA spectra (denoted as $PMF_{ambient+TD}$); this is the same approach applied in Huffman et al. (2009a). However, in this study we encountered several issues in $PMF_{ambient+TD}$ analysis. The first issue we encountered is the *mixing* behavior of OA factors. For example, in the three-factor solution of $PMF_{ambient+TD}$, one factor has similar fragmentation pattern as HOA from $PMF_{ambient}$, but this factor also has a substantial signal at $C_2H_4O_2^+$ (m/z 60, often used as a tracer marker for SFOA) (Fig. S6). In addition, another factor from $PMF_{ambient+TD}$ has similar time series as SFOA from $PMF_{ambient}$, but has similar mass spectrum as OOA from $PMF_{ambient}$. The second issue we encountered is that the mass loading of the OOA factor is occasionally higher in the TD runs compared to the preceding and succeeding bypass runs (Fig. S7). The reason for this behavior is not clear, but it is likely caused by the fact that only highly oxidized species remain upon heating and the mass spectrum of the remaining OA becomes more similar to the oxidized OA factors. Thus, PMF analysis might overestimate the concentrations of the oxidized OA factor. Overall, the PMF analysis on the combined bypass and TD line measurements by using the PMF2 solver without a priori information could not clearly separate OA factors. This is likely caused by the fact that including the thermally denuded data might distort the PMF results by introducing additional time variation in the mass spectra as pointed out by Huffman et al. (2009a).

Considering the above issues associated with $PMF_{ambient+TD}$, we performed PMF analysis using the ME-2 solver on the TD line measurements by applying the factor profiles determined from $PMF_{ambient}$ as a priori information, in order to improve the separation of OA factor. Data obtained at 120 and 250 °C were analyzed separately in order to account for the variability of factor mass spectra at different temperatures. The analyses for 120 and 250 °C are denoted as ME-2_{120C} and ME-2_{250C}, respectively, and were performed using the toolkit Source Finder (SoFi v4.8) (Canonaco et al., 2013). The error matrix was pre-treated in the same way as for $PMF_{ambient}$. As recommended by Canonaco et al. (2013) and Crippa et al. (2014), secondary factors (i.e., OOA factor) were unconstrained and primary factors (i.e., HOA and SFOA) were constrained with a small a value (e.g., < 0.1), which allows small variations of the resolved factors compared to the anchor profile in order to account for differences in ambient sources and avoid a mixing situation. We performed sensitivity tests and found that increasing the a value from 0 to 0.1 only reduced the fitting *residual* (i.e., Q/Q_{exp}) by < 1 % and had negligible influence on the factor profiles and factor concentrations (Figs. S8 and S9) for both ME-2_{120C} and ME-2_{250C}. Therefore, considering (1) the small effect of the a value, and (2) the fact that the anchor profiles of HOA and SFOA resolved from $PMF_{ambient}$ were clearly separated, we selected 0 as the a value, which fully constrained the profile of HOA and SFOA. The mass spectra of thermally denuded OOA at 120 and 250 °C, which were not constrained in ME-2_{120C} and ME-2_{250C}, change slightly compared to the ambient OOA mass spectrum (Fig. S10). The most

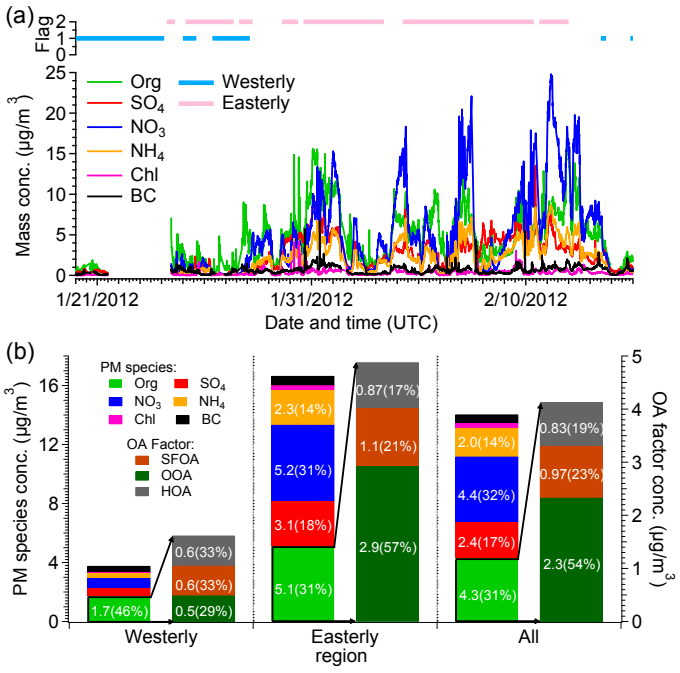

Figure 3. (a) Time series of non-refractory species and black carbon in addition to the flag waves of dominant air mass origin based on the NAME model. **(b)** Average concentration of non-refractory species, black carbon, and OA factors resolved by PMF analysis for the easterly sector, westerly sector, and the whole campaign. The unexplained mass by PMF analysis is less than 6 % of total OA and not shown in the figure. The gap between 1/22 and 1/25 is due to a clogged instrument inlet.

discernable changes occur at f_{CHO+} (i.e., fraction of organic signal at CHO^+), f_{C2H3O+}, and f_{CO2+}, suggesting that the composition of OOA is different at different denuding temperatures.

2.4.2 Retroplume analysis

Retroplume analysis was performed using the Numerical Atmospheric-Dispersion Modelling Environment (NAME) dispersion model (Jones et al., 2007) to identify the origin of air masses. The NAME model used the Unified Model reanalysis of meteorological data and generated the surface level pathways of air masses arriving at the site after 1 day of transport (i.e., 1-day footprints). The domain of influence of the NAME run was divided into a number of geographical regions (Atlantic ocean, Benelux area, etc; shown in Fig. S11) as described in Fleming et al. (2012). For each 3 h period, the fraction of air masses arriving from each region was calculated. According to Liu et al. (2013), for the time periods when the fraction of one region is greater than the 40th percentile of that region's air masses fraction, that region is deemed to have a strong influence on the sampling site. Regions can also be grouped into broader sectors. In this study, we focused on two broader sectors, the easterly sector (northern France and Benelux area) and the westerly sector (Atlantic and Ireland). It is important to note that sometimes the sampling site is influenced by more than one sector.

In the following discussion, we first investigate the PM_1 composition and OA source apportionment at the Detling site (Sect. 3.1). Then in Sect. 3.2, we compare the measurements at the rural Detling site with the urban NK site to investigate the spatial variability of aerosol in the greater London area. Lastly, we examine the aerosol volatility based on measurements at the Detling site (Sect. 3.3).

3 Results and discussion

3.1 Aerosol characterization at the Detling site

Figure 3a shows the time series of PM_1 composition measured by HR-ToF-AMS (i.e., non-refractory species) and SP2 (i.e., rBC). The campaign-averaged PM_1 concentration is $14 \pm 12\,\mu g\,m^{-3}$ (average $\pm$ 1 standard deviation). The chemical composition of PM_1 is dominated by nitrate and organics, which on average accounts for 32 and 31 % of total PM_1 mass, respectively. The other components include sulfate (17 %), ammonium (14 %), rBC (4.3 %), and chloride (2.2 %). Based on the fragmentation pattern of nitrate functionality in the AMS (i.e., NO^+/NO_2^+ ratio), one can determine whether the nitrate is of organic or inorganic origin (Farmer et al., 2010; Boyd et al., 2015; Fry et al., 2009; Xu et al., 2015b). At the Detling site, the measured NO^+/NO_2^+ ratio is close to the value of pure ammonium nitrate (Fig. S12),

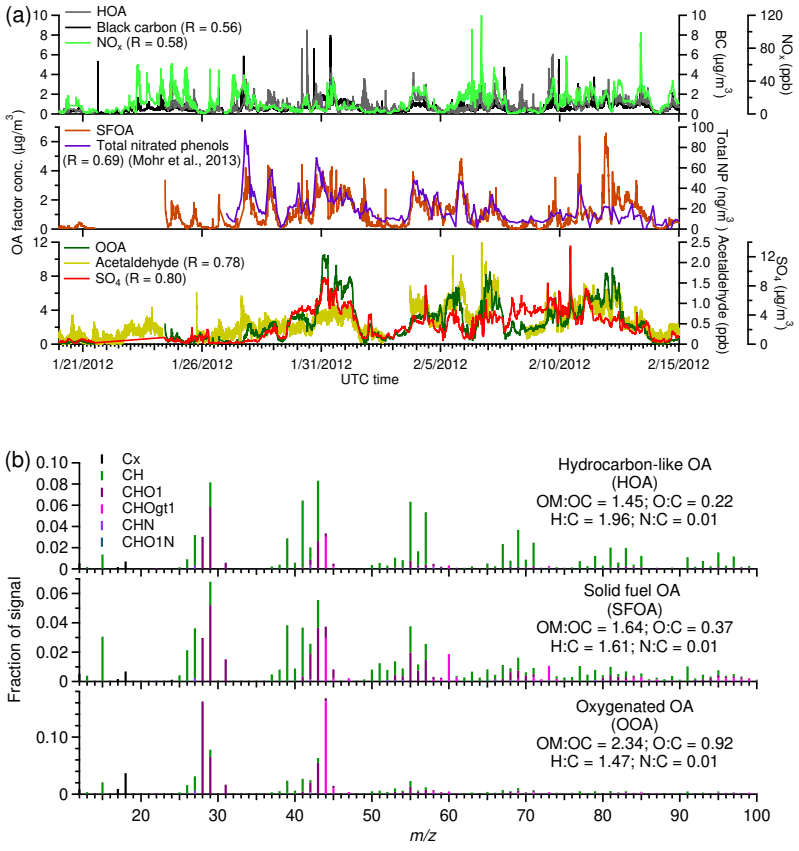

Figure 4. **(a)** Time series of OA factors resolved from the unconstrained PMF analysis on the ambient data (i.e., $PMF_{ambient}$) and corresponding external tracers. **(b)** Mass spectra of OA factors, which are colored by the ion type. The time series of total nitrated phenols is from Mohr et al. (2013).

indicating that the majority of the measured nitrates are inorganic nitrates.

The PMF analysis on the ambient organic mass spectra (i.e., $PMF_{ambient}$) resolves three OA subtypes: OOA, SFOA, and HOA, which accounts for 54, 23, and 19 % of total OA, respectively. The time series and mass spectra of the three factors are shown in Fig. 4. HOA is representative of primary OA from vehicle emissions as its mass spectrum is dominated by hydrocarbon-like ions (i.e., $C_xH_y^+$ ions). HOA is correlated with rBC and NO_x (Fig. 4a). SFOA is a surrogate for fresh OA from solid fuel combustion, including biomass burning (Young et al., 2015b). The mass spectrum of SFOA is characterized by prominent signals at $C_2H_4O_2^+$ (m/z 60) and $C_3H_5O_2^+$ (m/z 73), which are likely fragments from anhydrosugars such as levoglucosan and mannosan (tracers for biomass burning). The time series of SFOA correlates with particle-phase nitrated phenol compounds (Mohr et al., 2013), which are mainly associated with coal and wood combustion (Fig. 4b). OOA is the most oxidized (O : C = 0.92) among all three factors. At the Detling site, the OOA time series shows a good correlation with sulfate (Pearson's $R = 0.80$, Fig. 4a) and acetaldehyde ($R = 0.78$, Fig. 4a). Acetaldehyde could arise from direct emissions, such as fossil fuel combustion and biomass burning, and secondary production by oxidation of various hydrocarbons (Langford et al., 2009). The observation that acetaldehyde correlates better with OOA than SFOA ($R = 0.78$ vs. 0.66) is consistent with previous studies, which showed that acetaldehyde is dominated by secondary production after hours of photochemical processing (Hayes et al., 2013; Sommariva et al., 2011; de Gouw et al., 2005).

The identification of the sources of OOA is challenging because the mass spectrum of OA from different sources becomes more similar and resembles that of OOA with increasing photochemical aging (Ng et al., 2010; Jimenez et al., 2009). For the Detling data, we hypothesize that OOA is mainly from aged biomass burning. Liu et al. (2015) combined the PMF results from our study with radiocarbon analysis and estimated that 73–90 % of carbon in the OOA factor was non-fossil. Biogenic emissions and biomass burning are the major sources for non-fossil carbon. The large fraction of non-fossil carbon indicates that the OOA measured at the Detling site largely arises from aged biomass burning because the concentration of biogenic VOCs is low in win-

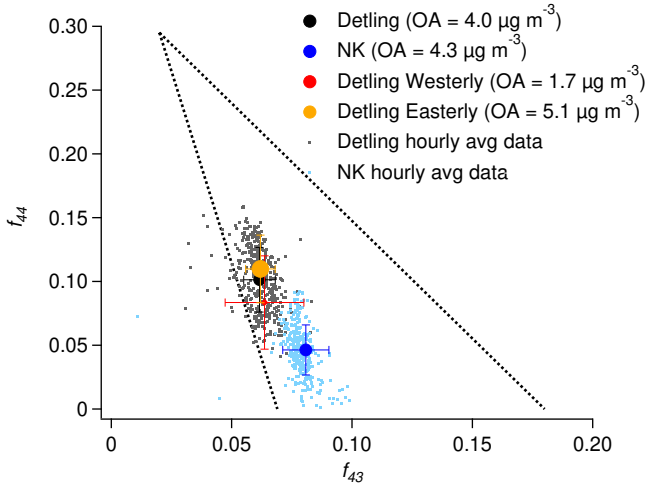

Figure 5. f_{44} vs. f_{43} for Detling and NK sites, as well as for the westerly sector and easterly sector of the Detling site. The dotted lines were adapted from Ng et al. (2010). The averages are sized by average organic loading. The error bars indicate 1 standard deviation. The average OA concentration at the Detling site is different from the value in Fig. 3 due to different sampling periods.

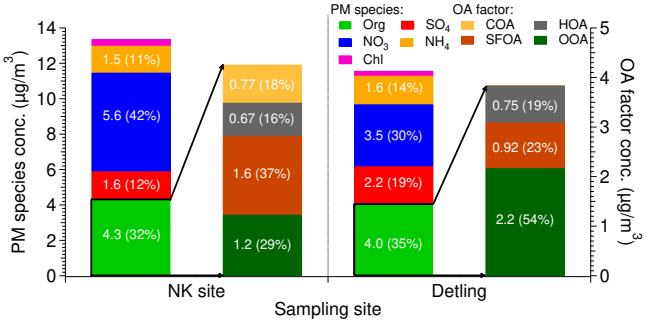

Figure 6. Comparison between NK and Detling sites in terms of the campaign-averaged concentration and mass fraction of non-refractory species and OA factors. The unexplained mass by PMF analysis is less than 6 % of total OA and not shown in the figure.

ter due to cold temperature and reduced photosynthesis. For example, Yin et al. (2015) showed that the concentrations of isoprene SOA tracers (i.e., methyltetrols) and α-pinene SOA tracers (pinic acid and pinonic acid) at the NK site during the winter IOP are only 0.5 and 2.3 ng m^{-3}, respectively, which are substantially lower than the concentrations measured at US and European sites during warmer months. Both laboratory studies and ambient measurements have revealed that the oxidation of biomass burning OA is a rapid process (Hennigan et al., 2011; May et al., 2012; Bougiatioti et al., 2014; Zhao et al., 2015). During the oxidation process, the mass spectrum of biomass burning OA could lose its characteristic signature (i.e., $C_2H_4O_2^+$ and $C_3H_5O_2^+$) and becomes progressively similar to that of OOA (Grieshop et al., 2009a; Hennigan et al., 2011). Thus, the aged biomass burning OA could be apportioned to the OOA by PMF analysis. With this, it is possible that the biomass burning OA contributes a larger fraction of ambient OA in winter than what previous field studies suggested, where the biomass burning OA was typically identified based on the presence of prominent signals at $C_2H_4O_2^+$ (m/z 60) and $C_3H_5O_2^+$ (m/z 73) alone.

Figure 3b shows the aerosol composition when air masses come from the easterly sector (i.e., mainland Europe) and the westerly sector (i.e., Atlantic Ocean). The concentration of PM_1 is 5 times higher for the easterly sector compared to the westerly sector. This is consistent with previous studies, which showed that elevated pollution levels in the southern UK were often associated with heavily polluted air masses transported from mainland Europe (Charron et al., 2013; Morgan et al., 2010, 2015; Putaud et al., 2004). Similar to the greater London area, Beekmann et al. (2015) found that 70 % of $PM_{2.5}$ mass in the Paris megacity was also largely influenced by regional contribution from mainland Europe. A large fraction of OA from mainland Europe is highly oxidized organic aerosol (i.e., OOA). For example, while the concentrations of HOA and SFOA only double when the source of air masses switches from the Atlantic Ocean to mainland Europe, the OOA concentration increases from $\sim$0.5 to $\sim$3 μg m^{-3} (Fig. 3b). The higher contribution of OOA to total OA is consistent with the total OA from mainland Europe being more oxidized than that from the Atlantic Ocean. In Fig. 5, we compare the OA oxidation level for different air masses in the f_{44} (i.e., fraction of organic signal at m/z 44) vs. f_{43} (i.e., fraction of organic signal at m/z 43) plot (Ng et al., 2010). The OA for the easterly sector has a higher f_{44} compared to the westerly sector, suggesting that the air masses advected from mainland Europe have undergone a larger extent of photochemical processing.

3.2 Comparison between London and Detling

In this section, we compare the two simultaneous HR-ToF-AMS measurements at the rural Detling site and the urban NK site. Only the sampling periods (hourly basis) when both instruments were operative from 20 January to 8 February, 2012, are included in the comparison; therefore, that the concentrations reported in this section are different from those reported in Sect. 3.1, where the whole data set at the Detling site (from 20 January to 15 February, 2012) is used.

3.2.1 Non-refractory species and OA factors comparison

The comparison between the Detling and NK sites in terms of concentration and diurnal variation of the five NR-PM_1 species is shown in Figs. 6 and S13, respectively. The concentration of nitrate is substantially higher at the urban NK site (i.e., 5.6 μg m^{-3}) than the rural Detling site (3.5 μg m^{-3}). This observation is consistent with McMeeking et al. (2012), who performed airborne measurements in the urban London

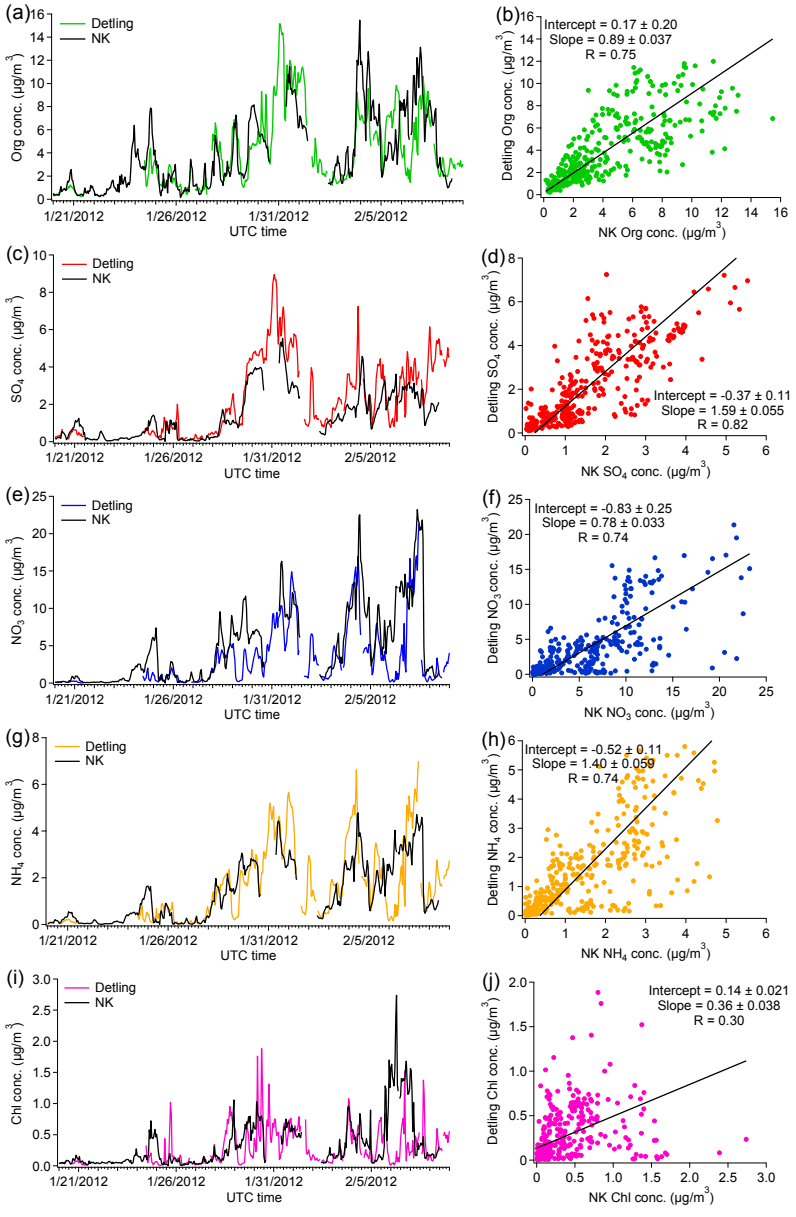

Figure 7. Comparison of non-refractory species time series between NK and Detling sites. The intercept and slope are obtained by orthogonal distance regression. The Pearson's R is obtained by linear least-squares fit.

region and observed an enhancement of nitrate concentration inside urban plumes. The elevated nitrate concentration (largely inorganic nitrate) at the urban site suggests that nitrate has a strong local contribution, likely due to the fact that nitrate formation occurs rapidly and its major sources (i.e., oxidation of NO_x) are much higher over inner London (Shaw et al., 2015). The sulfate concentration is well-correlated between two sites ($R = 0.82$, Fig. 7), consistent with previous findings that sulfate has a strong regional contribution in the greater London area (Harrison et al., 2012; Yin et al., 2010). However, the sulfate concentration is about 60 % higher at the rural Detling site than the urban NK site. The comparison of sulfate concentration between the rural and urban site depends on the origin of air masses. As shown in Fig. S14, the sulfate concentrations agree well between the two sites when air masses come from Atlantic Ocean (i.e., westerly) compared to mainland Europe (i.e., easterly). The reason for the elevated sulfate concentration at the rural site will be discussed below.

Although the average concentration of total OA is comparable between NK (i.e., 4.3 μg m^{-3}) and Detling (4.0 μg m^{-3}) (Fig. 6), PMF analysis reveals that the contribution to total OA from different sources is distinctly different between the urban and rural sites. At the urban NK site, primary OA

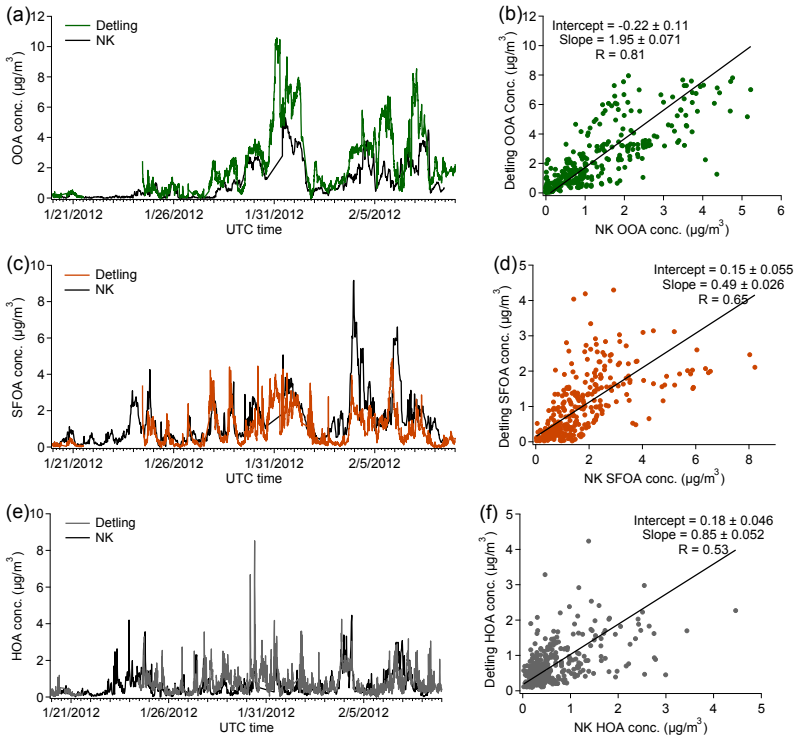

Figure 8. Comparison of OA factors time series between NK and Detling sites. The intercept and slope are obtained by orthogonal distance regression. The Pearson's R is obtained by linear least-squares fit.

sources, including cooking, vehicle emissions, and solid fuel combustion, account for about 70 % of total OA. At the rural Detling site, in contrast, more than half of the total OA is aged secondary OA (i.e., OOA). Specifically, the cooking OA (i.e., COA), which accounts for 18 % of total OA at the urban NK site, is not resolved at the rural Detling site. This is expected as there is no cooking activity near the rural Detling site. Hydrocarbon-like OA (i.e., HOA) only shows weak correlation between the two sites ($R = 0.53$) (Fig. 8f), which is because HOA is representative of primary OA and it is influenced by local vehicle emissions. The SFOA time series is moderately correlated ($R = 0.65$) between Detling and NK (Fig. 8d). The SFOA concentration at the urban NK site is almost twice as high at the rural Detling site, which is likely due to the elevated domestic space heating activities and related emissions in the urban London area during wintertime (Young et al., 2015b; Crilley et al., 2015).

Among all three OA factors, the OOA factor has the strongest correlation between the two sites ($R = 0.81$) (Fig. 8b), which suggests that OOA likely represents regional SOA. Crilley et al. (2015) also observed that the filter-based daily-averaged OC concentration is well-correlated ($R^2 > 0.82$) between Detling and NK sites during the same period as our study. However, the good correlations of OOA and OC observed in our study and Crilley et al. (2015) are different from the observation in Charron et al. (2013), where the authors found that secondary organic carbon (SOC) was much less spatially homogeneous than nitrate and sulfate by comparing an urban (Birmingham site) and a rural site (Harwell site) in the greater London area between July and November 2010. The difference between this study and Charron et al. (2013) is likely due to the uncertainty in the SOC estimation method. In Charron et al. (2013), SOC is estimated from filter measured total OC by using the EC / OC method where a constant EC / CC ratio from primary sources is applied. As discussed in Charron et al. (2013), their estimation and the weak correlation of OC between different sites are affected by the uncertainties associated with the choice of source ratios and analytical procedure. In addition to SOC estimation uncertainty, the differences in sampling sites, sampling periods, and size cuts ($PM_{2.5}$ vs. PM_1) between Charron et al. (2013) and our study could also play a role.

Although the OOA is well-correlated between the two sites, the OOA concentration is almost twice as high at the rural Detling site than the urban NK site (Fig. 6). This observation is similar to the comparison of sulfate between the two sites, which is also usually considered to be regional, as discussed above. Based on atmospheric chemistry transport model, the higher OOA concentration at the rural site is a result of meteorological conditions, which cause a strong gradient of SOA concentration when air masses are advected from polluted mainland Europe. For example, to simulate the SOA formation in the winter IOP, Ots et al. (2016) applied the regional EMEP4UK (European Monitoring and Evalu-

ation Programme) model, which uses 5 km by 5 km British Isles grid nested within 50 km by 50 km greater Europe domain, 21 vertical levels, Weather Research and Forecasting (WRF) model meteorological reanalysis, National Atmospheric Emissions Inventory (NAEI) for the UK, and Centre on Emission Inventories and Projections (CEIP) emissions for other European countries. They observed a steep negative gradient of SOA concentration from near-European continent to southern England. The steep gradient is a result of meteorological conditions (i.e., mainly wind direction), which causes that the pollution plume from mainland Europe largely passes over the rural site, but not the urban site.

3.2.2 OA oxidation level

Figure 5 compares the OA oxidation level between Detling and NK. Compared to the NK site, the average OA at the Detling site has higher f_{44}, indicating that the OA at the Detling site is more oxidized than that at the NK site. The difference in OA oxidation level between the Detling and the NK sites are due to different OA compositions. As shown in Fig. 6, the OA at the NK site is dominated by primary OA ($\sim$ 70 % of total OA) from cooking, vehicle emissions, and solid fuel combustion, whose O : C is much lower than OOA. In contrast, more than half of OA at the Detling site is OOA, which is highly oxidized.

3.3 Aerosol volatility analysis

3.3.1 Volatility of non-refractory species and OA factors

Figure 9a and c show the thermograms and the change in concentration after heating (ΔC) of non-refractory (NR) species as measured by the HR-ToF-AMS. The MFR is calculated as the ratio of the species mass concentration through the TD to the average mass concentration of the preceding and succeeding bypass runs. The ΔC is calculated as the concentration difference between the bypass and TD runs (Eq. 4). Both the MFR and the ΔC have been corrected for the particle loss in the TD by using the TD transmission efficiency as discussed in Sect. 2.2. The MFR of NR species is consistent with previous ambient measurements (Huffman et al., 2009a). Nitrate has the largest average ΔC and the smallest MFR among all NR species. The MFR of nitrate decreases to 0.15 at 120 °C and it volatilizes completely at 250 °C (i.e., MFR < 0.05). Sulfate is the least volatile species at 120 °C, which has the smallest average ΔC and an MFR equal to 0.89. The sulfate MFR is higher than that of ammonium sulfate from laboratory studies, which has been attributed to particle mixing state affecting the sulfate volatility (Huffman et al., 2009a; Massoli et al., 2015). For OA, the MFR is about 0.16 at 250 °C. On average, 0.88 µg m^{-3} OA remains after heating, implying the existence of non-volatile organic compounds. Figure 9d shows that the ΔCs of three OA factors

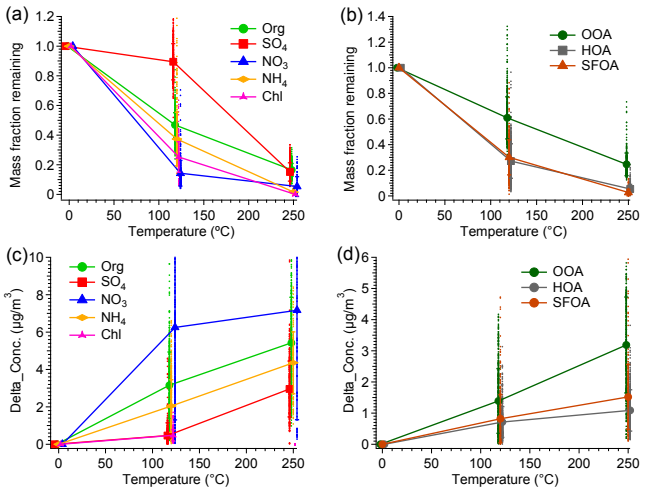

Figure 9. Thermogram of **(a)** non-refractory species and **(b)** OA factors. The change in mass concentration after heating in the TD (i.e., ΔC) of **(c)** non-refractory species and **(d)** OA factors. Error bars indicate 1 standard deviation. The average values are connected by lines to guide the eyes.

are not statistically different at 120 °C. This suggests that although the O : C of OOA (O : C = 0.92) is substantially larger than that of HOA (O : C = 0.22) and SFOA (O : C = 0.37), the volatilities of the three factors are similar at 120 °C. Thus, the O : C may not be a good indicator of the volatility of the OA factors. At 250 °C, both HOA and SFOA fully evaporate (MFR < 0.05) so that the volatility cannot be compared under this temperature.

3.3.2 Sources of residual organics at 250 °C

Figure 10 shows the chemical composition of the residual PM_1 after heating to 250 °C. The major components of the residual PM_1 are OA (90 % of OA is OOA), rBC, and sulfate. rBC accounts for about 30 % of the remaining mass. This value is smaller than that reported in Poulain et al. (2014) (i.e., 47 % in summer and 59 % in winter for TD temperature 300 °C) and in Häkkinen et al. (2012) (i.e., 55–87 % depending on season for TD temperature 280 °C). The differences are likely due to (1) the density of rBC used in previous studies when converting SMPS volume concentration to mass concentration, (2) different TD temperatures and residence times, (3) techniques to measure rBC concentration, and (4) sampling locations.

At 250 °C, OA has the largest contribution ($\sim$ 40 %) to the residual mass. The existence of highly oxidized, non-volatile organic compounds is consistent with previous ambient measurements and model studies. For example, Cappa and Jimenez (2010) used a kinetic model to simulate the volatility of OA factors measured by Huffman et al. (2009a) in the MILAGRO field campaign and the authors estimated

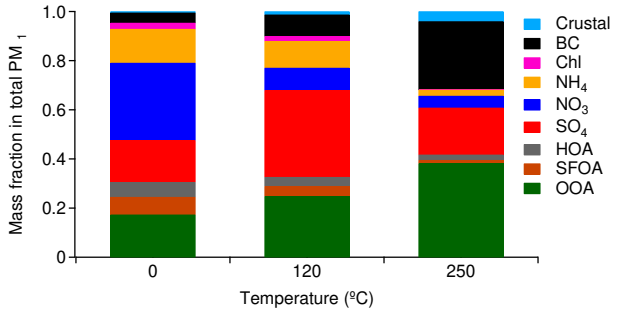

Figure 10. Mass fraction of PM_1 species for bypass line and TD line (i.e., 120 and 250 °C). The mass fractions larger than 9 % are labeled in the figure.

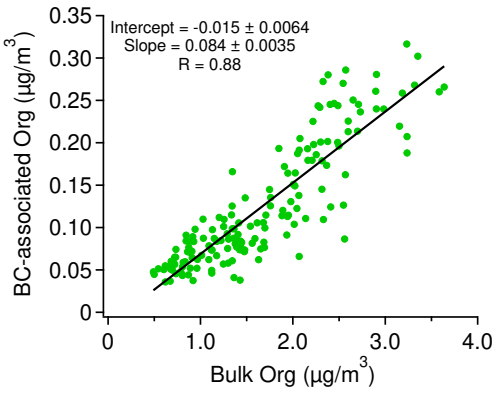

Figure 11. Comparison between organics associated with rBC (measured by SP-AMS with laser vaporizer only) and the non-refractory organics in the bulk measurement (by HR-ToF-AMS) after heating at 250 °C.

that a large fraction of OA was non-volatile and would not evaporate under any atmospheric conditions.

The sources of non-volatile organics are uncertain, but appear to be related to anthropogenic emissions. A previous study by Häkkinen et al. (2012) showed that the MFR (excluding rBC) at 280 °C correlated well with anthropogenic tracers (i.e., polycyclic aromatic hydrocarbons), indicating that the non-volatile species may be affected by anthropogenic emissions. In this study, we investigate the sources of the non-volatile organics by comparing the measurements of HR-ToF-AMS and SP-AMS after heating at 250 °C. While the HR-ToF-AMS measures the bulk total non-refractory organics, SP-AMS only detects the organics associated with rBC when the SP-AMS is operated with the laser vaporizer only (i.e., no tungsten vaporizer) (Onasch et al., 2012). Figure 11 shows that after heating at 250 °C, the residual organics associated with rBC correlate well with the residual organics in the bulk measurements, and they only account for < 10 % of the bulk measurements. Therefore, this good correlation is not caused by a large contribution from rBC-associated species, but is possibly caused by the fact that the non-volatile organics in the bulk measurements have similar sources or have undergone similar chemical processing as rBC in the atmosphere. Denkenberger et al. (2007) suggested that the non-volatile organics may be oligomers formed within the TD based on the observation that oligomer intensity increased after heating ambient particles in a TD. In our study, the signals at high m/z (100–180), which are potential indicators for oligomers, decrease with TD temperature (Fig. S15). This suggests that the non-volatile organics are unlikely to be oligomers formed within the TD.

3.3.3 OA MFR and O : C ratio

To examine the relationship between O : C and MFR, the O : C of thermally denuded OA is plotted as a function of TD temperature. As shown in Fig. 12a, the O : C of thermally denuded OA increases with increasing TD temperature, indicating that the residual OA with lower volatility is more oxidized, which is consistent with previous observations (Huffman et al., 2009a, b). Thus, it appears that the OA oxidation level (i.e., O : C) is correlated with MFR. If so, one would expect that ambient OA with higher O : C should have larger MFR. However, as shown in Fig. 12b to e, the MFR increases only slightly with the bypass O : C (or OS) over a wide range of O : C (or OS). In addition, the correlation between MFR and bypass O : C (or OS) is weak (i.e., $R < 0.4$), suggesting that the volatility of OA cannot be readily inferred by its O : C or OS.

The lack of correlation between OA MFR and O : C is likely due to the distributions of volatility and O : C in bulk OA; that is, one population of particles with a higher bulk O : C could have lower MFR after heating compared to another population of particles with a lower bulk O : C, if the volatility and O : C distributions are different between two populations. In the following discussion, we use a simple model to illustrate our point (Fig. 13). Two populations of particles are comprised of three compounds (i.e., A, B, and C), but with different amounts. These three compounds have the same molecular weight, but different volatility and O : C. The assumed properties of the three compounds and the compositions of two populations of particles are atmospherically relevant and are summarized in Fig. 13. Although the average O : C of population no. 2 (i.e., 0.75) is higher than that of population no. 1 (i.e., 0.61), population no. 2 has the same MFR as population no. 1 after heating, which is consistent with the trend in Fig. 12b–e. On the other hand, the O : C of each population always increases after heating, which is consistent

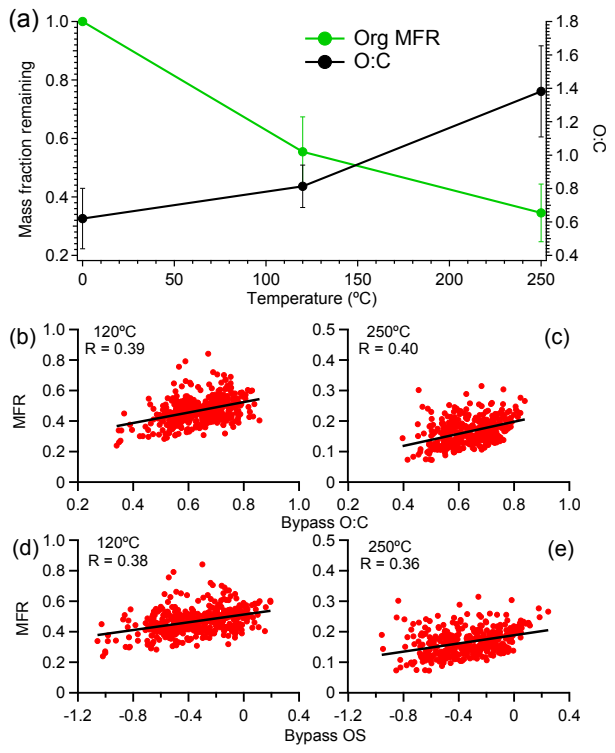

Figure 12. (a) Organic mass fraction remaining (MFR) and O : C as a function of TD temperature; **(b–e)** organic MFR at 120 and 250 °C as a function of bypass line organic O : C and oxidation state.

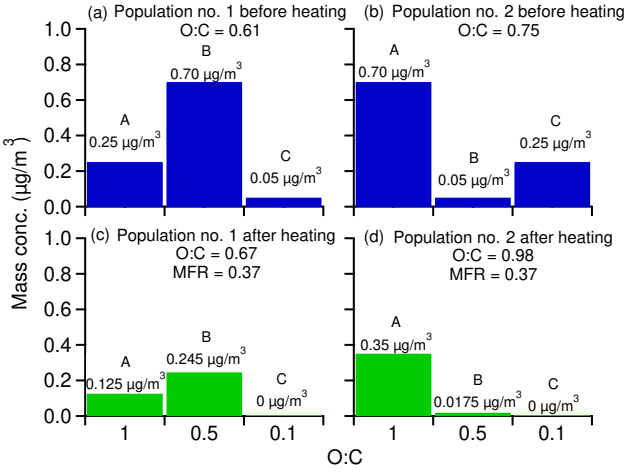

Figure 13. The properties (O : C and volatility) of three model compounds and the composition of two populations of particles used in the simple model to illustrate the relationship between bulk OA O : C and volatility. The O : C is 1, 0.5, and 0.1 for compound A, B, and C, respectively. Upon heating at temperature T0, 50, 65, and 100 % of A, B, and C would evaporate. Population no. 1 is comprised of 0.25, 0.7, and 0.05 µg m^{-3} of A, B, and C, respectively, and population no. 2 is comprised of 0.7, 0.05, and 0.25 µg m^{-3} of A, B, and C, respectively.

with the observation in Fig. 12a. We note that the example described here is specific; however, it clearly illustrates that the distributions of volatility and O : C largely influence the relationship between O : C and MFR of bulk OA. This also helps to explain the various types of relationship between O : C and MFR observed in laboratory studies (Grieshop et al., 2009b; Qi et al., 2010; Donahue et al., 2012; Kroll et al., 2009; Tritscher et al., 2011; Xu et al., 2014). In previous laboratory studies, while the SOA generally becomes progressively more oxidized (i.e., O : C increases) during the chemical aging, the volatility distribution evolves differently for different SOA systems, which results in various types of MFR trends (i.e., increases, or stays constant, or decreases over time). Our analysis emphasizes the importance of understanding the distribution of volatility and O : C in bulk OA and reveals the potential weakness of using one averaged O : C value to describe the degree of oxidation, which is in line with the two-dimensional volatility-oxidation modeling framework proposed by Donahue et al. (2011). In addition to the distribution of O : C and volatility, the fact that MFR depends on the initial concentration of OA, which is different between studies, may also contribute to the various relationships between O : C and MFR.

Hildebrandt et al. (2010) proposed that the lack of correlation between O : C and volatility in Finokalia, Greece, was caused by the OA being highly oxidized with an average O : C of 0.8 (estimated from the measured f_{44}). In order to test this hypothesis, we plot the O : C enhancement (i.e., ratio between O : C of thermally denuded OA and O : C of ambient OA) vs. O : C of ambient OA (Fig. 14a) to show the O : C enhancement after heating. By extrapolating the linear fit under different temperatures, we find that if the O : C of ambient OA is about 1, the enhancement is negligible even after heating at 250 °C. It is important to note that the O : C reported in Fig. 14a is calculated based on the recent formulation in Canagaratna et al. (2015). The improved O : C calculation method in Canagaratna et al. (2015) results in higher O : C compared to the values based on Aiken et al. (2008), which was used in Hildebrandt et al. (2010). By using the method in Aiken et al. (2008), we found that the O : C threshold for no enhancement is 0.8 (Fig. S16), which is the same as the O : C of ambient OA in Hildebrandt et al. (2010). In addition, the campaign-averaged f_{44} of ambient OA in Hildebrandt et al. (2010) is 0.182, which is close to f_{44} of TD OA under 250 °C (i.e., 0.188) in our study (Fig. 14b). To conclude, this analysis provides a specific case in which the average O : C ratio might not be a good indicator of OA volatility.

4 Conclusions

In this study, we deployed a suite of instruments to characterize the composition of PM_1 at a rural site (Detling, Kent) near London during the Clean Air for London (ClearfLo) project

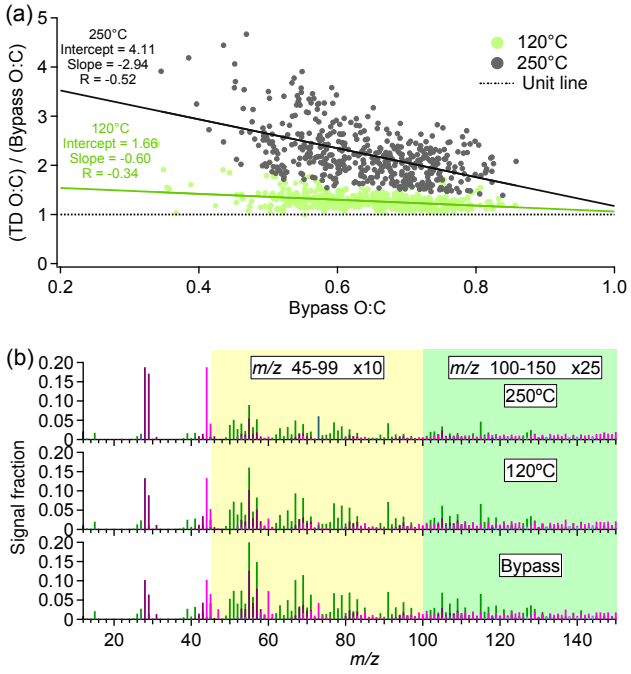

Figure 14. **(a)** O : C enhancement (i.e., ratio of TD line O : C to bypass line O : C) as a function of bypass line O : C. **(b)** Mass spectra of OA under different TD temperatures. The signals between m/z 45 and 99 are multiplied by 10 and the signals between m/z 100 and 150 are multiplied by 25 for clarity. The mass spectra are colored by the ion type in the same way as Fig. 4b.

in 2012 winter. Nitrate and organics are two major components in PM_1, each of which accounts for $\sim 30\,\%$ of total PM_1 mass concentration. Retroplume analysis reveals that the PM_1 concentration in the greater London area is largely influenced by the origin of the air masses. When air masses are advected from mainland Europe, the PM_1 concentration is elevated and the organic aerosol is more oxidized. Oxygenated organic aerosol (OOA) accounts for $\sim 50\,\%$ of total OA. Taking advantage of measurements in winter when the biogenic emissions are low, we hypothesize that the OOA in the current study is likely aged OA from biomass burning. The hypothesis is based on the combined PMF and radiocarbon analysis where more than 70 % of carbon in OOA is estimated to be non-fossil (Liu et al., 2015) and cannot be explained by the small amount of biogenic SOA in winter.

With simultaneous HR-ToF-AMS measurements taking place at the rural Detling site and the urban North Kensington site, we have a unique opportunity to investigate the spatial variability of PM_1 in the greater London area. The nitrate concentration is markedly higher at the urban site compared to the rural site (i.e., 5.6 vs. 3.5 $\mu g\,m^{-3}$). The high nitrate concentration at the rural site together with the urban excess of nitrate imply that the nitrate in the greater London area has a high regional background overlaid by important contributions from local production. Although the OA concentration is comparable between the rural and urban sites, PMF analysis suggests distinctly different contribution from different sources between the two sites. Similar to previous studies, we find that OA at the urban site mainly arises from primary sources, while OA at the rural site is mainly secondary. Vehicle emission, solid fuel combustion, and cooking together account for $\sim 70\,\%$ of OA at the urban NK site. In contrast, OOA contributes more than half of total OA at the rural Detling site. Among all OA factors, OOA has the best correlation between the two sites ($R = 0.81$), which suggests that this factor is largely regional. We find that the OOA concentration is almost twice as high at the rural Detling site than the urban NK site. This is a result of meteorological conditions, which cause a strong gradient of SOA concentration when air masses are advected from polluted mainland Europe. The observation that the OOA concentration is higher at the rural site than urban site is opposite to the trend shown in Zhang et al. (2007). However, the trend reported in Zhang et al. (2007) is not based on simultaneous measurements at paired rural and urban sites. Thus, our observation highlights the importance of meteorology in determining the OA spatial distribution.

A TD was deployed to investigate the volatility of PM_1 species at the Detling site. We find that although OOA has substantial larger O : C than HOA and SFOA, the volatilities of these three factors are similar at 120 °C, which is inferred from the change in mass concentration after heating at 120 °C. This suggests that the O : C may not be a good proxy for OA factor volatility. We note that 16 % of total OA remains even after heating at 250 °C, suggesting the existence of non-volatile organics. PMF analysis reveals that the majority of the remaining organics are oxygenated OA. At 250 °C, the time series of the residual organics measured by HR-ToF-AMS correlate well with the residual organics associated with rBC measured by SP-AMS. The good correlation suggests that the non-volatile organics likely have similar sources or have undergone similar chemical processing as rBC in the atmosphere, considering that rBC-associated organics only account for < 10 % of bulk organics.

We evaluate the relationship between the volatility (using the MFR) and degree of oxidation (using the O : C or OS) of bulk OA. We found that, on the one hand, the O : C of thermally denuded OA is higher than that of ambient OA, indicating that less-volatile compounds have higher O : C. On the other hand, the MFR of OA shows a weak correlation with O : C of ambient OA, indicating that the average O : C of bulk OA may not be a good indicator for volatility. One possible explanation for the seemingly contradictory observations lies in the broad distribution of volatility and O : C in bulk OA. For example, different O : C distributions could result in the same bulk O : C but different volatility distributions, which may cause particles with the same O : C to have different MFR. Thus, it is important to understand and use the distribution of properties (i.e., the distribution of volatility and O : C) to describe the complexity of OA.

The Supplement related to this article is available online at doi:10.5194/acp-16-1139-2016-supplement.

Acknowledgements. This project was supported by the US Department of Energy (grant no. DE-SC000602) and in part by the UK Natural Environment Research Council (NERC) ClearfLo project (grant ref. NE/H008136/1), coordinated by the National Centre for Atmospheric Science (NCAS). D.E. Young acknowledges a NERC PhD studentship (ref. NE/I528142/1). A.C. Aiken acknowledges Director's postdoctoral funding from LANL's LDRD program. M.K. Dubey acknowledges support by the US DOE Office of Biological and Environmental Research Atmospheric System Research Program, F265 to LANL. Elemental analysis was funded by the Swiss National Science Foundation (grant nos. 200021_132467/1 and 200020_150056) and the European Community's Seventh Framework Programme (FP7/2007-2013; grant no. 312284). The authors would like to thank the Met Office for use of the NAME dispersion model and the Meteorological data used in it and for the Leicester University ALICE supercomputer for running the model. The authors gratefully acknowledge Ashley Williamson (DOE), Amon Haruta (Los Alamos National Laboratory), David Green (Kings College London), and Roger Moore (Kent County Showgrounds) for assistance with the organization of the field site in Detling, UK. Processed and quality assured data are available through the ClearfLo project archive at the British Atmospheric Data Centre (http://badc.nerc.ac.uk/browse/badc/clearflo) and through the US Department of Energy Atmospheric Radiation Measurement Archive (www.archive.arm.gov). Raw data are archived at the Georgia Institute of Technology and at Aerodyne Research, Inc. and are available on request.

Edited by: B. Ervens

References

Aiken, A. C., DeCarlo, P. F., and Jimenez, J. L.: Elemental Analysis of Organic Species with Electron Ionization High-Resolution Mass Spectrometry, Anal. Chem., 79, 8350–8358, doi:10.1021/ac071150w, 2007.

Aiken, A. C., Decarlo, P. F., Kroll, J. H., Worsnop, D. R., Huffman, J. A., Docherty, K. S., Ulbrich, I. M., Mohr, C., Kimmel, J. R., Sueper, D., Sun, Y., Zhang, Q., Trimborn, A., Northway, M., Ziemann, P. J., Canagaratna, M. R., Onasch, T. B., Alfarra, M. R., Prevot, A. S. H., Dommen, J., Duplissy, J., Metzger, A., Baltensperger, U., and Jimenez, J. L.: O / C and OM / OC ratios of primary, secondary, and ambient organic aerosols with high-resolution time-of-flight aerosol mass spectrometry, Environ. Sci. Technol., 42, 4478–4485, doi:10.1021/Es703009q, 2008.

An, W. J., Pathak, R. K., Lee, B. H., and Pandis, S. N.: Aerosol volatility measurement using an improved thermodenuder: Application to secondary organic aerosol, J. Aerosol. Sci., 38, 305–314, doi:10.1016/j.jaerosci.2006.12.002, 2007.

Baumgardner, D., Popovicheva, O., Allan, J., Bernardoni, V., Cao, J., Cavalli, F., Cozic, J., Diapouli, E., Eleftheriadis, K., Genberg, P. J., Gonzalez, C., Gysel, M., John, A., Kirchstetter, T. W., Kuhlbusch, T. A. J., Laborde, M., Lack, D., Müller, T., Niessner, R., Petzold, A., Piazzalunga, A., Putaud, J. P., Schwarz, J., Sheridan, P., Subramanian, R., Swietlicki, E., Valli, G., Vecchi, R., and Viana, M.: Soot reference materials for instrument calibration and intercomparisons: a workshop summary with recommendations, Atmos. Meas. Tech., 5, 1869–1887, doi:10.5194/amt-5-1869-2012, 2012.

Beekmann, M., Prévôt, A. S. H., Drewnick, F., Sciare, J., Pandis, S. N., Denier van der Gon, H. A. C., Crippa, M., Freutel, F., Poulain, L., Ghersi, V., Rodriguez, E., Beirle, S., Zotter, P., von der Weiden-Reinmüller, S.-L., Bressi, M., Fountoukis, C., Petetin, H., Szidat, S., Schneider, J., Rosso, A., El Haddad, I., Megaritis, A., Zhang, Q. J., Michoud, V., Slowik, J. G., Moukhtar, S., Kolmonen, P., Stohl, A., Eckhardt, S., Borbon, A., Gros, V., Marchand, N., Jaffrezo, J. L., Schwarzenboeck, A., Colomb, A., Wiedensohler, A., Borrmann, S., Lawrence, M., Baklanov, A., and Baltensperger, U.: In situ, satellite measurement and model evidence on the dominant regional contribution to fine particulate matter levels in the Paris megacity, Atmos. Chem. Phys., 15, 9577–9591, doi:10.5194/acp-15-9577-2015, 2015.

Bohnenstengel, S. I., Belcher, S. E., Aiken, A., Allan, J. D., Allen, G., Bacak, A., Bannan, T. J., Barlow, J. F., Beddows, D. C. S., Bloss, W. J., Booth, A. M., Chemel, C., Coceal, O., Di Marco, C. F., Dubey, M. K., Faloon, K. H., Fleming, Z. L., Furger, M., Gietl, J. K., Graves, R. R., Green, D. C., Grimmond, C. S. B., Halios, C. H., Hamilton, J. F., Harrison, R. M., Heal, M. R., Heard, D. E., Helfter, C., Herndon, S. C., Holmes, R. E., Hopkins, J. R., Jones, A. M., Kelly, F. J., Kotthaus, S., Langford, B., Lee, J. D., Leigh, R. J., Lewis, A. C., Lidster, R. T., Lopez-Hilfiker, F. D., McQuaid, J. B., Mohr, C., Monks, P. S., Nemitz, E., Ng, N. L., Percival, C. J., Prévôt, A. S. H., Ricketts, H. M. A., Sokhi, R., Stone, D., Thornton, J. A., Tremper, A. H., Valach, A. C., Visser, S., Whalley, L. K., Williams, L. R., Xu, L., Young, D. E., and Zotter, P.: Meteorology, Air Quality, and Health in London: The ClearfLo Project, B. Am. Meteorol. Soc., 96, 779–804, doi:10.1175/BAMS-D-12-00245.1, 2014.

Bougiatioti, A., Stavroulas, I., Kostenidou, E., Zarmpas, P., Theodosi, C., Kouvarakis, G., Canonaco, F., Prévôt, A. S. H., Nenes, A., Pandis, S. N., and Mihalopoulos, N.: Processing of biomass-burning aerosol in the eastern Mediterranean during summertime, Atmos. Chem. Phys., 14, 4793–4807, doi:10.5194/acp-14-4793-2014, 2014.

Boyd, C. M., Sanchez, J., Xu, L., Eugene, A. J., Nah, T., Tuet, W. Y., Guzman, M. I., and Ng, N. L.: Secondary organic aerosol formation from the β-pinene + NO_3 system: effect of humidity and peroxy radical fate, Atmos. Chem. Phys., 15, 7497–7522, doi:10.5194/acp-15-7497-2015, 2015.

Canagaratna, M. R., Jayne, J. T., Jimenez, J. L., Allan, J. D., Alfarra, M. R., Zhang, Q., Onasch, T. B., Drewnick, F., Coe, H., Middlebrook, A., Delia, A., Williams, L. R., Trimborn, A. M., Northway, M. J., DeCarlo, P. F., Kolb, C. E., Davidovits, P., and Worsnop, D. R.: Chemical and microphysical characterization of ambient aerosols with the aerodyne aerosol mass spectrometer, Mass Spectrom. Rev., 26, 185–222, doi:10.1002/mas.20115, 2007.

Canagaratna, M. R., Jimenez, J. L., Kroll, J. H., Chen, Q., Kessler, S. H., Massoli, P., Hildebrandt Ruiz, L., Fortner, E., Williams, L. R., Wilson, K. R., Surratt, J. D., Donahue, N. M., Jayne, J. T., and Worsnop, D. R.: Elemental ratio measurements of organic

compounds using aerosol mass spectrometry: characterization, improved calibration, and implications, Atmos. Chem. Phys., 15, 253–272, doi:10.5194/acp-15-253-2015, 2015.

Canonaco, F., Crippa, M., Slowik, J. G., Baltensperger, U., and Prévôt, A. S. H.: SoFi, an IGOR-based interface for the efficient use of the generalized multilinear engine (ME-2) for the source apportionment: ME-2 application to aerosol mass spectrometer data, Atmos. Meas. Tech., 6, 3649–3661, doi:10.5194/amt-6-3649-2013, 2013.

Cappa, C. D. and Jimenez, J. L.: Quantitative estimates of the volatility of ambient organic aerosol, Atmos. Chem. Phys., 10, 5409–5424, doi:10.5194/acp-10-5409-2010, 2010.

Charron, A., Degrendele, C., Laongsri, B., and Harrison, R. M.: Receptor modelling of secondary and carbonaceous particulate matter at a southern UK site, Atmos. Chem. Phys., 13, 1879–1894, doi:10.5194/acp-13-1879-2013, 2013.

Crilley, L. R., Bloss, W. J., Yin, J., Beddows, D. C. S., Harrison, R. M., Allan, J. D., Young, D. E., Flynn, M., Williams, P., Zotter, P., Prevot, A. S. H., Heal, M. R., Barlow, J. F., Halios, C. H., Lee, J. D., Szidat, S., and Mohr, C.: Sources and contributions of wood smoke during winter in London: assessing local and regional influences, Atmos. Chem. Phys., 15, 3149–3171, doi:10.5194/acp-15-3149-2015, 2015.

Crippa, M., DeCarlo, P. F., Slowik, J. G., Mohr, C., Heringa, M. F., Chirico, R., Poulain, L., Freutel, F., Sciare, J., Cozic, J., Di Marco, C. F., Elsasser, M., Nicolas, J. B., Marchand, N., Abidi, E., Wiedensohler, A., Drewnick, F., Schneider, J., Borrmann, S., Nemitz, E., Zimmermann, R., Jaffrezo, J.-L., Prévôt, A. S. H., and Baltensperger, U.: Wintertime aerosol chemical composition and source apportionment of the organic fraction in the metropolitan area of Paris, Atmos. Chem. Phys., 13, 961–981, doi:10.5194/acp-13-961-2013, 2013.

Crippa, M., Canonaco, F., Lanz, V. A., Äijälä, M., Allan, J. D., Carbone, S., Capes, G., Ceburnis, D., Dall'Osto, M., Day, D. A., DeCarlo, P. F., Ehn, M., Eriksson, A., Freney, E., Hildebrandt Ruiz, L., Hillamo, R., Jimenez, J. L., Junninen, H., Kiendler-Scharr, A., Kortelainen, A.-M., Kulmala, M., Laaksonen, A., Mensah, A. A., Mohr, C., Nemitz, E., O'Dowd, C., Ovadnevaite, J., Pandis, S. N., Petäjä, T., Poulain, L., Saarikoski, S., Sellegri, K., Swietlicki, E., Tiitta, P., Worsnop, D. R., Baltensperger, U., and Prévôt, A. S. H.: Organic aerosol components derived from 25 AMS data sets across Europe using a consistent ME-2 based source apportionment approach, Atmos. Chem. Phys., 14, 6159–6176, doi:10.5194/acp-14-6159-2014, 2014.

DeCarlo, P. F., Kimmel, J. R., Trimborn, A., Northway, M. J., Jayne, J. T., Aiken, A. C., Gonin, M., Fuhrer, K., Horvath, T., Docherty, K. S., Worsnop, D. R., and Jimenez, J. L.: Field-Deployable, High-Resolution, Time-of-Flight Aerosol Mass Spectrometer, Anal. Chem., 78, 8281–8289, doi:10.1021/ac061249n, 2006.

de Gouw, J. A., Middlebrook, A. M., Warneke, C., Goldan, P. D., Kuster, W. C., Roberts, J. M., Fehsenfeld, F. C., Worsnop, D. R., Canagaratna, M. R., Pszenny, A. A. P., Keene, W. C., Marchewka, M., Bertman, S. B., and Bates, T. S.: Budget of organic carbon in a polluted atmosphere: Results from the New England Air Quality Study in 2002, J. Geophys. Res.-Atmos., 110, D16305, doi:10.1029/2004jd005623, 2005.

Denkenberger, K. A., Moffet, R. C., Holecek, J. C., Rebotier, T. P., and Prather, K. A.: Real-Time, Single-Particle Measurements of Oligomers in Aged Ambient Aerosol Particles, Environ. Sci. Technol., 41, 5439–5446, doi:10.1021/es070329l, 2007.

Donahue, N. M., Epstein, S. A., Pandis, S. N., and Robinson, A. L.: A two-dimensional volatility basis set: 1. organic-aerosol mixing thermodynamics, Atmos. Chem. Phys., 11, 3303–3318, doi:10.5194/acp-11-3303-2011, 2011.

Donahue, N. M., Henry, K. M., Mentel, T. F., Kiendler-Scharr, A., Spindler, C., Bohn, B., Brauers, T., Dorn, H. P., Fuchs, H., Tillmann, R., Wahner, A., Saathoff, H., Naumann, K. H., Mohler, O., Leisner, T., Muller, L., Reinnig, M. C., Hoffmann, T., Salo, K., Hallquist, M., Frosch, M., Bilde, M., Tritscher, T., Barmet, P., Praplan, A. P., DeCarlo, P. F., Dommen, J., Prevot, A. S. H., and Baltensperger, U.: Aging of biogenic secondary organic aerosol via gas-phase OH radical reactions, P. Natl. Acad. Sci. USA, 109, 13503–13508, doi:10.1073/pnas.1115186109, 2012.

Farmer, D. K., Matsunaga, A., Docherty, K. S., Surratt, J. D., Seinfeld, J. H., Ziemann, P. J., and Jimenez, J. L.: Response of an aerosol mass spectrometer to organonitrates and organosulfates and implications for atmospheric chemistry, P. Natl. Acad. Sci., 107, 6670–6675, doi:10.1073/pnas.0912340107, 2010.

Fleming, Z. L., Monks, P. S., and Manning, A. J.: Review: Untangling the influence of air-mass history in interpreting observed atmospheric composition, Atmos. Res., 104–105, 1–39, doi:10.1016/j.atmosres.2011.09.009, 2012.

Fry, J. L., Kiendler-Scharr, A., Rollins, A. W., Wooldridge, P. J., Brown, S. S., Fuchs, H., Dubé, W., Mensah, A., dal Maso, M., Tillmann, R., Dorn, H.-P., Brauers, T., and Cohen, R. C.: Organic nitrate and secondary organic aerosol yield from NO_3 oxidation of β-pinene evaluated using a gas-phase kinetics/aerosol partitioning model, Atmos. Chem. Phys., 9, 1431–1449, doi:10.5194/acp-9-1431-2009, 2009.

Grieshop, A. P., Donahue, N. M., and Robinson, A. L.: Laboratory investigation of photochemical oxidation of organic aerosol from wood fires 2: analysis of aerosol mass spectrometer data, Atmos. Chem. Phys., 9, 2227–2240, doi:10.5194/acp-9-2227-2009, 2009a.

Grieshop, A. P., Logue, J. M., Donahue, N. M., and Robinson, A. L.: Laboratory investigation of photochemical oxidation of organic aerosol from wood fires 1: measurement and simulation of organic aerosol evolution, Atmos. Chem. Phys., 9, 1263–1277, doi:10.5194/acp-9-1263-2009, 2009b.

Häkkinen, S. A. K., Äijälä, M., Lehtipalo, K., Junninen, H., Backman, J., Virkkula, A., Nieminen, T., Vestenius, M., Hakola, H., Ehn, M., Worsnop, D. R., Kulmala, M., Petäjä, T., and Riipinen, I.: Long-term volatility measurements of submicron atmospheric aerosol in Hyytiälä, Finland, Atmos. Chem. Phys., 12, 10771–10786, doi:10.5194/acp-12-10771-2012, 2012.

Hallquist, M., Wenger, J. C., Baltensperger, U., Rudich, Y., Simpson, D., Claeys, M., Dommen, J., Donahue, N. M., George, C., Goldstein, A. H., Hamilton, J. F., Herrmann, H., Hoffmann, T., Iinuma, Y., Jang, M., Jenkin, M. E., Jimenez, J. L., Kiendler-Scharr, A., Maenhaut, W., McFiggans, G., Mentel, Th. F., Monod, A., Prévôt, A. S. H., Seinfeld, J. H., Surratt, J. D., Szmigielski, R., and Wildt, J.: The formation, properties and impact of secondary organic aerosol: current and emerging issues, Atmos. Chem. Phys., 9, 5155–5236, doi:10.5194/acp-9-5155-2009, 2009.

Harrison, R. M., Dall'Osto, M., Beddows, D. C. S., Thorpe, A. J., Bloss, W. J., Allan, J. D., Coe, H., Dorsey, J. R., Gallagher,

M., Martin, C., Whitehead, J., Williams, P. I., Jones, R. L., Langridge, J. M., Benton, A. K., Ball, S. M., Langford, B., Hewitt, C. N., Davison, B., Martin, D., Petersson, K. F., Henshaw, S. J., White, I. R., Shallcross, D. E., Barlow, J. F., Dunbar, T., Davies, F., Nemitz, E., Phillips, G. J., Helfter, C., Di Marco, C. F., and Smith, S.: Atmospheric chemistry and physics in the atmosphere of a developed megacity (London): an overview of the REPARTEE experiment and its conclusions, Atmos. Chem. Phys., 12, 3065–3114, doi:10.5194/acp-12-3065-2012, 2012.

Hayes, P. L., Ortega, A. M., Cubison, M. J., Froyd, K. D., Zhao, Y., Cliff, S. S., Hu, W. W., Toohey, D. W., Flynn, J. H., Lefer, B. L., Grossberg, N., Alvarez, S., Rappenglueck, B., Taylor, J. W., Allan, J. D., Holloway, J. S., Gilman, J. B., Kuster, W. C., De Gouw, J. A., Massoli, P., Zhang, X., Liu, J., Weber, R. J., Corrigan, A. L., Russell, L. M., Isaacman, G., Worton, D. R., Kreisberg, N. M., Goldstein, A. H., Thalman, R., Waxman, E. M., Volkamer, R., Lin, Y. H., Surratt, J. D., Kleindienst, T. E., Offenberg, J. H., Dusanter, S., Griffith, S., Stevens, P. S., Brioude, J., Angevine, W. M., and Jimenez, J. L.: Organic aerosol composition and sources in Pasadena, California, during the 2010 CalNex campaign, J. Geophys. Res.-Atmos., 118, 9233–9257, doi:10.1002/Jgrd.50530, 2013.

Hennigan, C. J., Miracolo, M. A., Engelhart, G. J., May, A. A., Presto, A. A., Lee, T., Sullivan, A. P., McMeeking, G. R., Coe, H., Wold, C. E., Hao, W.-M., Gilman, J. B., Kuster, W. C., de Gouw, J., Schichtel, B. A., Collett Jr., J. L., Kreidenweis, S. M., and Robinson, A. L.: Chemical and physical transformations of organic aerosol from the photo-oxidation of open biomass burning emissions in an environmental chamber, Atmos. Chem. Phys., 11, 7669–7686, doi:10.5194/acp-11-7669-2011, 2011.

Hildebrandt, L., Engelhart, G. J., Mohr, C., Kostenidou, E., Lanz, V. A., Bougiatioti, A., DeCarlo, P. F., Prevot, A. S. H., Baltensperger, U., Mihalopoulos, N., Donahue, N. M., and Pandis, S. N.: Aged organic aerosol in the Eastern Mediterranean: the Finokalia Aerosol Measurement Experiment – 2008, Atmos. Chem. Phys., 10, 4167–4186, doi:10.5194/acp-10-4167-2010, 2010.

Hildebrandt Ruiz, L., Paciga, A. L., Cerully, K. M., Nenes, A., Donahue, N. M., and Pandis, S. N.: Formation and aging of secondary organic aerosol from toluene: changes in chemical composition, volatility, and hygroscopicity, Atmos. Chem. Phys., 15, 8301–8313, doi:10.5194/acp-15-8301-2015, 2015.

Huang, X.-F., He, L.-Y., Hu, M., Canagaratna, M. R., Sun, Y., Zhang, Q., Zhu, T., Xue, L., Zeng, L.-W., Liu, X.-G., Zhang, Y.-H., Jayne, J. T., Ng, N. L., and Worsnop, D. R.: Highly time-resolved chemical characterization of atmospheric submicron particles during 2008 Beijing Olympic Games using an Aerodyne High-Resolution Aerosol Mass Spectrometer, Atmos. Chem. Phys., 10, 8933–8945, doi:10.5194/acp-10-8933-2010, 2010.

Huffman, J. A., Ziemann, P. J., Jayne, J. T., Worsnop, D. R., and Jimenez, J. L.: Development and Characterization of a Fast-Stepping/Scanning Thermodenuder for Chemically-Resolved Aerosol Volatility Measurements, Aerosol. Sci. Tech., 42, 395–407, doi:10.1080/02786820802104981, 2008.

Huffman, J. A., Docherty, K. S., Aiken, A. C., Cubison, M. J., Ulbrich, I. M., DeCarlo, P. F., Sueper, D., Jayne, J. T., Worsnop, D. R., Ziemann, P. J., and Jimenez, J. L.: Chemically-resolved aerosol volatility measurements from two megacity field studies, Atmos. Chem. Phys., 9, 7161–7182, doi:10.5194/acp-9-7161-2009, 2009a.

Huffman, J. A., Docherty, K. S., Mohr, C., Cubison, M. J., Ulbrich, I. M., Ziemann, P. J., Onasch, T. B., and Jimenez, J. L.: Chemically-Resolved Volatility Measurements of Organic Aerosol from Different Sources, Environ. Sci. Technol., 43, 5351–5357, doi:10.1021/es803539d, 2009b.

Jimenez, J. L., Canagaratna, M. R., Donahue, N. M., Prevot, A. S. H., Zhang, Q., Kroll, J. H., DeCarlo, P. F., Allan, J. D., Coe, H., Ng, N. L., Aiken, A. C., Docherty, K. S., Ulbrich, I. M., Grieshop, A. P., Robinson, A. L., Duplissy, J., Smith, J. D., Wilson, K. R., Lanz, V. A., Hueglin, C., Sun, Y. L., Tian, J., Laaksonen, A., Raatikainen, T., Rautiainen, J., Vaattovaara, P., Ehn, M., Kulmala, M., Tomlinson, J. M., Collins, D. R., Cubison, M. J., Dunlea, E. J., Huffman, J. A., Onasch, T. B., Alfarra, M. R., Williams, P. I., Bower, K., Kondo, Y., Schneider, J., Drewnick, F., Borrmann, S., Weimer, S., Demerjian, K., Salcedo, D., Cottrell, L., Griffin, R., Takami, A., Miyoshi, T., Hatakeyama, S., Shimono, A., Sun, J. Y., Zhang, Y. M., Dzepina, K., Kimmel, J. R., Sueper, D., Jayne, J. T., Herndon, S. C., Trimborn, A. M., Williams, L. R., Wood, E. C., Middlebrook, A. M., Kolb, C. E., Baltensperger, U., and Worsnop, D. R.: Evolution of Organic Aerosols in the Atmosphere, Science, 326, 1525–1529, doi:10.1126/science.1180353, 2009.

Jones, A., Thomson, D., Hort, M., and Devenish, B.: The UK Met Office's Next-Generation Atmospheric Dispersion Model, NAME III, in: Air Pollution Modeling and Its Application XVII, edited by: Borrego, C. and Norman, A.-L., Springer US, USA, 580–589, 2007.

Jonsson, A. M., Hallquist, M., and Saathoff, H.: Volatility of secondary organic aerosols from the ozone initiated oxidation of alpha-pinene and limonene, J. Aerosol Sci., 38, 843–852, doi:10.1016/j.jaerosci.2007.06.008, 2007.

Kroll, J. H., Smith, J. D., Che, D. L., Kessler, S. H., Worsnop, D. R., and Wilson, K. R.: Measurement of fragmentation and functionalization pathways in the heterogeneous oxidation of oxidized organic aerosol, Phys. Chem. Chem. Phys., 11, 8005–8014, doi:10.1039/B905289e, 2009.

Kuwata, M., Zorn, S. R., and Martin, S. T.: Using Elemental Ratios to Predict the Density of Organic Material Composed of Carbon, Hydrogen, and Oxygen, Environ. Sci. Technol., 46, 787–794, doi:10.1021/es202525q, 2012.

Laborde, M., Mertes, P., Zieger, P., Dommen, J., Baltensperger, U., and Gysel, M.: Sensitivity of the Single Particle Soot Photometer to different black carbon types, Atmos. Meas. Tech., 5, 1031–1043, doi:10.5194/amt-5-1031-2012, 2012.

Langford, B., Davison, B., Nemitz, E., and Hewitt, C. N.: Mixing ratios and eddy covariance flux measurements of volatile organic compounds from an urban canopy (Manchester, UK), Atmos. Chem. Phys., 9, 1971–1987, doi:10.5194/acp-9-1971-2009, 2009.

Lanz, V. A., Alfarra, M. R., Baltensperger, U., Buchmann, B., Hueglin, C., and Prévôt, A. S. H.: Source apportionment of submicron organic aerosols at an urban site by factor analytical modelling of aerosol mass spectra, Atmos. Chem. Phys., 7, 1503–1522, doi:10.5194/acp-7-1503-2007, 2007.

Lee, B. H., Pierce, J. R., Engelhart, G. J., and Pandis, S. N.: Volatility of secondary organic aerosol from the ozonol-

ysis of monoterpenes, Atmos. Environ., 45, 2443–2452, doi:10.1016/j.atmosenv.2011.02.004, 2011.

Lide, D. R.: CRC Handbook of Chemistry and Physics, CRC Press Inc, USA, 1991.

Liu, D., Allan, J., Whitehead, J., Young, D., Flynn, M., Coe, H., McFiggans, G., Fleming, Z. L., and Bandy, B.: Ambient black carbon particle hygroscopic properties controlled by mixing state and composition, Atmos. Chem. Phys., 13, 2015–2029, doi:10.5194/acp-13-2015-2013, 2013.

Liu, S., Aiken, A. C., Gorkowski, K., Dubey, M. K., Cappa, C. D., Williams, L. R., Herndon, S. C., Massoli, P., Fortner, E. C., Chhabra, P. S., Brooks, W. A., Onasch, T. B., Jayne, J. T., Worsnop, D. R., China, S., Sharma, N., Mazzoleni, C., Xu, L., Ng, N. L., Liu, D., Allan, J. D., Lee, J. D., Fleming, Z. L., Mohr, C., Zotter, P., Szidat, S., and Prevot, A. S. H.: Enhanced light absorption by mixed source black and brown carbon particles in UK winter, Nat. Commun., 6, 8435, doi:10.1038/ncomms9435, 2015.

Malm, W. C., Sisler, J. F., Huffman, D., Eldred, R. A., and Cahill, T. A.: Spatial and seasonal trends in particle concentration and optical extinction in the United States, J. Geophys. Res.-Atmos., 99, 1347–1370, doi:10.1029/93JD02916, 1994.

Massoli, P., Onasch, T. B., Cappa, C. D., Nuamaan, I., Hakala, J., Hayden, K., Li, S.-M., Sueper, D. T., Bates, T. S., Quinn, P. K., Jayne, J. T., and Worsnop, D. R.: Characterization of black carbon-containing particles from soot particle aerosol mass spectrometer measurements on the R/V *Atlantis* during CalNex 2010, J. Geophys. Res.-Atmos., 120, 2575–2593, doi:10.1002/2014JD022834, 2015.

May, A. A., Saleh, R., Hennigan, C. J., Donahue, N. M., and Robinson, A. L.: Volatility of Organic Molecular Markers Used for Source Apportionment Analysis: Measurements and Implications for Atmospheric Lifetime, Environ. Sci. Technol., 46, 12435–12444, doi:10.1021/es302276t, 2012.

McMeeking, G. R., Bart, M., Chazette, P., Haywood, J. M., Hopkins, J. R., McQuaid, J. B., Morgan, W. T., Raut, J.-C., Ryder, C. L., Savage, N., Turnbull, K., and Coe, H.: Airborne measurements of trace gases and aerosols over the London metropolitan region, Atmos. Chem. Phys., 12, 5163–5187, doi:10.5194/acp-12-5163-2012, 2012.

Middlebrook, A. M., Bahreini, R., Jimenez, J. L., and Canagaratna, M. R.: Evaluation of Composition-Dependent Collection Efficiencies for the Aerodyne Aerosol Mass Spectrometer using Field Data, Aerosol Sci. Tech., 46, 258–271, doi:10.1080/02786826.2011.620041, 2012.

Mohr, C., DeCarlo, P. F., Heringa, M. F., Chirico, R., Slowik, J. G., Richter, R., Reche, C., Alastuey, A., Querol, X., Seco, R., Peñuelas, J., Jiménez, J. L., Crippa, M., Zimmermann, R., Baltensperger, U., and Prévôt, A. S. H.: Identification and quantification of organic aerosol from cooking and other sources in Barcelona using aerosol mass spectrometer data, Atmos. Chem. Phys., 12, 1649–1665, doi:10.5194/acp-12-1649-2012, 2012.

Mohr, C., Lopez-Hilfiker, F. D., Zotter, P., Prévôt, A. S. H., Xu, L., Ng, N. L., Herndon, S. C., Williams, L. R., Franklin, J. P., Zahniser, M. S., Worsnop, D. R., Knighton, W. B., Aiken, A. C., Gorkowski, K. J., Dubey, M. K., Allan, J. D., and Thornton, J. A.: Contribution of Nitrated Phenols to Wood Burning Brown Carbon Light Absorption in Detling, United Kingdom during Winter Time, Environ. Sci. Technol., 47, 6316–6324, doi:10.1021/es400683v, 2013.

Morgan, W. T., Allan, J. D., Bower, K. N., Highwood, E. J., Liu, D., McMeeking, G. R., Northway, M. J., Williams, P. I., Krejci, R., and Coe, H.: Airborne measurements of the spatial distribution of aerosol chemical composition across Europe and evolution of the organic fraction, Atmos. Chem. Phys., 10, 4065–4083, doi:10.5194/acp-10-4065-2010, 2010.

Morgan, W. T., Ouyang, B., Allan, J. D., Aruffo, E., Di Carlo, P., Kennedy, O. J., Lowe, D., Flynn, M. J., Rosenberg, P. D., Williams, P. I., Jones, R., McFiggans, G. B., and Coe, H.: Influence of aerosol chemical composition on N_2O_5 uptake: airborne regional measurements in northwestern Europe, Atmos. Chem. Phys., 15, 973–990, doi:10.5194/acp-15-973-2015, 2015.

Ng, N. L., Canagaratna, M. R., Zhang, Q., Jimenez, J. L., Tian, J., Ulbrich, I. M., Kroll, J. H., Docherty, K. S., Chhabra, P. S., Bahreini, R., Murphy, S. M., Seinfeld, J. H., Hildebrandt, L., Donahue, N. M., DeCarlo, P. F., Lanz, V. A., Prévôt, A. S. H., Dinar, E., Rudich, Y., and Worsnop, D. R.: Organic aerosol components observed in Northern Hemispheric datasets from Aerosol Mass Spectrometry, Atmos. Chem. Phys., 10, 4625–4641, doi:10.5194/acp-10-4625-2010, 2010.

Onasch, T. B., Trimborn, A., Fortner, E. C., Jayne, J. T., Kok, G. L., Williams, L. R., Davidovits, P., and Worsnop, D. R.: Soot Particle Aerosol Mass Spectrometer: Development, Validation, and Initial Application, Aerosol Sci. Tech., 46, 804–817, doi:10.1080/02786826.2012.663948, 2012.

Ots, R., Young, D. E., Vieno, M., Xu, L., Dunmore, R. E., Allan, J. D., Coe, H., Williams, L. R., Herndon, S. C., Ng, N. L., Hamilton, J. F., Bergström, R., Di Marco, C., Nemitz, E., Mackenzie, I. A., Kuenen, J. J. P., Green, D. C., Reis, S., and Heal, M. R.: Simulating secondary organic aerosol from missing diesel-related intermediate-volatility organic compound emissions during the Clean Air for London (ClearfLo) campaign, Atmos. Chem. Phys. Discuss., doi:10.5194/acp-2015-920, in review, 2016.

Paatero, P.: A weighted non-negative least squares algorithm for three-way "PARAFAC" factor analysis, Chemometr. Intell. Lab., 38, 223–242, doi:10.1016/S0169-7439(97)00031-2, 1997.

Paatero, P.: The Multilinear Engine – A Table-Driven, Least Squares Program for Solving Multilinear Problems, Including the n-Way Parallel Factor Analysis Model, J. Comput. Graph. Stat., 8, 854–888, doi:10.1080/10618600.1999.10474853, 1999.

Paatero, P. and Tapper, U.: Positive Matrix Factorization – a Nonnegative Factor Model with Optimal Utilization of Error-Estimates of Data Values, Environmetrics, 5, 111–126, doi:10.1002/env.3170050203, 1994.

Paciga, A., Karnezi, E., Kostenidou, E., Hildebrandt, L., Psichoudaki, M., Engelhart, G. J., Lee, B.-H., Crippa, M., Prévôt, A. S. H., Baltensperger, U., and Pandis, S. N.: Volatility of organic aerosol and its components in the Megacity of Paris, Atmos. Chem. Phys. Discuss., 15, 22263–22289, doi:10.5194/acpd-15-22263-2015, 2015.

Park, K., Cao, F., Kittelson, D. B., and McMurry, P. H.: Relationship between Particle Mass and Mobility for Diesel Exhaust Particles, Environ. Sci. Technol., 37, 577–583, doi:10.1021/es025960v, 2003.

Park, K., Kittelson, D., Zachariah, M., and McMurry, P.: Measurement of Inherent Material Density of Nanopar-

ticle Agglomerates, J. Nanopart. Res., 6, 267–272, doi:10.1023/B:NANO.0000034657.71309.e6, 2004.

Poulain, L., Birmili, W., Canonaco, F., Crippa, M., Wu, Z. J., Nordmann, S., Spindler, G., Prévôt, A. S. H., Wiedensohler, A., and Herrmann, H.: Chemical mass balance of 300 °C non-volatile particles at the tropospheric research site Melpitz, Germany, Atmos. Chem. Phys., 14, 10145–10162, doi:10.5194/acp-14-10145-2014, 2014.

Putaud, J.-P., Raes, F., Van Dingenen, R., Brüggemann, E., Facchini, M. C., Decesari, S., Fuzzi, S., Gehrig, R., Hüglin, C., Laj, P., Lorbeer, G., Maenhaut, W., Mihalopoulos, N., Müller, K., Querol, X., Rodriguez, S., Schneider, J., Spindler, G., Brink, H. t., Tørseth, K., and Wiedensohler, A.: A European aerosol phenomenology – 2: chemical characteristics of particulate matter at kerbside, urban, rural and background sites in Europe, Atmos. Environ., 38, 2579–2595, doi:10.1016/j.atmosenv.2004.01.041, 2004.

Qi, L., Nakao, S., Malloy, Q., Warren, B., and Cocker, D. R.: Can secondary organic aerosol formed in an atmospheric simulation chamber continuously age?, Atmos. Environ., 44, 2990–2996, doi:10.1016/j.atmosenv.2010.05.020, 2010.

Riipinen, I., Pierce, J. R., Donahue, N. M., and Pandis, S. N.: Equilibration time scales of organic aerosol inside thermodenuders: Evaporation kinetics versus thermodynamics, Atmos. Environ., 44, 597–607, doi:10.1016/j.atmosenv.2009.11.022, 2010.

Salcedo, D., Onasch, T. B., Dzepina, K., Canagaratna, M. R., Zhang, Q., Huffman, J. A., DeCarlo, P. F., Jayne, J. T., Mortimer, P., Worsnop, D. R., Kolb, C. E., Johnson, K. S., Zuberi, B., Marr, L. C., Volkamer, R., Molina, L. T., Molina, M. J., Cardenas, B., Bernabé, R. M., Márquez, C., Gaffney, J. S., Marley, N. A., Laskin, A., Shutthanandan, V., Xie, Y., Brune, W., Lesher, R., Shirley, T., and Jimenez, J. L.: Characterization of ambient aerosols in Mexico City during the MCMA-2003 campaign with Aerosol Mass Spectrometry: results from the CENICA Supersite, Atmos. Chem. Phys., 6, 925–946, doi:10.5194/acp-6-925-2006, 2006.

Saleh, R., Shihadeh, A., and Khlystov, A.: On transport phenomena and equilibration time scales in thermodenuders, Atmos. Meas. Tech., 4, 571–581, doi:10.5194/amt-4-571-2011, 2011.

Saleh, R., Khlystov, A., and Shihadeh, A.: Determination of Evaporation Coefficients of Ambient and Laboratory-Generated Semivolatile Organic Aerosols from Phase Equilibration Kinetics in a Thermodenuder, Aerosol Sci. Tech., 46, 22–30, doi:10.1080/02786826.2011.602762, 2012.

Schwarz, J. P., Gao, R. S., Fahey, D. W., Thomson, D. S., Watts, L. A., Wilson, J. C., Reeves, J. M., Darbeheshti, M., Baumgardner, D. G., Kok, G. L., Chung, S. H., Schulz, M., Hendricks, J., Lauer, A., Karcher, B., Slowik, J. G., Rosenlof, K. H., Thompson, T. L., Langford, A. O., Loewenstein, M., and Aikin, K. C.: Single-particle measurements of midlatitude black carbon and light-scattering aerosols from the boundary layer to the lower stratosphere, J. Geophys. Res.-Atmos., 111, D16207, doi:10.1029/2006jd007076, 2006.

Shaw, M. D., Lee, J. D., Davison, B., Vaughan, A., Purvis, R. M., Harvey, A., Lewis, A. C., and Hewitt, C. N.: Airborne determination of the temporo-spatial distribution of benzene, toluene, nitrogen oxides and ozone in the boundary layer across Greater London, UK, Atmos. Chem. Phys., 15, 5083–5097, doi:10.5194/acp-15-5083-2015, 2015.

Sommariva, R., de Gouw, J. A., Trainer, M., Atlas, E., Goldan, P. D., Kuster, W. C., Warneke, C., and Fehsenfeld, F. C.: Emissions and photochemistry of oxygenated VOCs in urban plumes in the Northeastern United States, Atmos. Chem. Phys., 11, 7081–7096, doi:10.5194/acp-11-7081-2011, 2011.

Stanier, C. O., Pathak, R. K., and Pandis, S. N.: Measurements of the volatility of aerosols from alpha-piniene ozonolysis, Environ. Sci. Technol., 41, 2756–2763, doi:10.1021/Es0519280, 2007.

Stephens, M., Turner, N., and Sandberg, J.: Particle identification by laser-induced incandescence in a solid-state laser cavity, Appl. Optics, 42, 3726–3736, doi:10.1364/Ao.42.003726, 2003.

Tang, M. J., Shiraiwa, M., Pöschl, U., Cox, R. A., and Kalberer, M.: Compilation and evaluation of gas phase diffusion coefficients of reactive trace gases in the atmosphere: Volume 2. Diffusivities of organic compounds, pressure-normalised mean free paths, and average Knudsen numbers for gas uptake calculations, Atmos. Chem. Phys., 15, 5585–5598, doi:10.5194/acp-15-5585-2015, 2015.

Tritscher, T., Dommen, J., DeCarlo, P. F., Gysel, M., Barmet, P. B., Praplan, A. P., Weingartner, E., Prévôt, A. S. H., Riipinen, I., Donahue, N. M., and Baltensperger, U.: Volatility and hygroscopicity of aging secondary organic aerosol in a smog chamber, Atmos. Chem. Phys., 11, 11477–11496, doi:10.5194/acp-11-11477-2011, 2011.

Ulbrich, I. M., Canagaratna, M. R., Zhang, Q., Worsnop, D. R., and Jimenez, J. L.: Interpretation of organic components from Positive Matrix Factorization of aerosol mass spectrometric data, Atmos. Chem. Phys., 9, 2891–2918, doi:10.5194/acp-9-2891-2009, 2009.

Visser, S., Slowik, J. G., Furger, M., Zotter, P., Bukowiecki, N., Dressler, R., Flechsig, U., Appel, K., Green, D. C., Tremper, A. H., Young, D. E., Williams, P. I., Allan, J. D., Herndon, S. C., Williams, L. R., Mohr, C., Xu, L., Ng, N. L., Detournay, A., Barlow, J. F., Halios, C. H., Fleming, Z. L., Baltensperger, U., and Prévôt, A. S. H.: Kerb and urban increment of highly time-resolved trace elements in PM_{10}, $PM_{2.5}$ and $PM_{1.0}$ winter aerosol in London during ClearfLo 2012, Atmos. Chem. Phys., 15, 2367–2386, doi:10.5194/acp-15-2367-2015, 2015.

Williams, L., Herndon, S., Jayne, J., Freedman, A., Brooks, B., Franklin, J. P., Massoli, P., Fortner, E., Chhabra, P. S., Zahniser, M. S., Stark, H., canagaratna, M., Onasch, T., Worsnop, D., Ng, N. L., Xu, L., Knighton, B., Aiken, A., Gorkowski, K. J., Liu, S., Martin, A. T., Coulter, R., Lopez-Hilfiker, F. D., Mohr, C., Thornton, J., Visser, S., Furger, M., Zotter, P., and Prevot, A. S. H.: Characterization of black carbon containing particles in rural wintertime UK with an Aerodyne soot particle aerosol mass spectrometer (SP-AMS), Atmos. Chem. Phys. Discuss., in preparation, 2016.

Xu, L., Kollman, M. S., Song, C., Shilling, J. E., and Ng, N. L.: Effects of NO_x on the Volatility of Secondary Organic Aerosol from Isoprene Photooxidation, Environ. Sci. Technol., 48, 2253–2262, doi:10.1021/es404842g, 2014.

Xu, L., Guo, H., Boyd, C. M., Klein, M., Bougiatioti, A., Cerully, K. M., Hite, J. R., Isaacman-VanWertz, G., Kreisberg, N. M., Knote, C., Olson, K., Koss, A., Goldstein, A. H., Hering, S. V., de Gouw, J., Baumann, K., Lee, S.-H., Nenes, A., Weber, R. J., and Ng, N. L.: Effects of anthropogenic emissions on aerosol formation from isoprene and monoterpenes in the southeastern United States,

P. Natl. Acad. Sci., 112, 37–42, doi:10.1073/pnas.1417609112, 2015a.

Xu, L., Suresh, S., Guo, H., Weber, R. J., and Ng, N. L.: Aerosol characterization over the southeastern United States using high-resolution aerosol mass spectrometry: spatial and seasonal variation of aerosol composition and sources with a focus on organic nitrates, Atmos. Chem. Phys., 15, 7307–7336, doi:10.5194/acp-15-7307-2015, 2015b.

Yin, J., Harrison, R. M., Chen, Q., Rutter, A., and Schauer, J. J.: Source apportionment of fine particles at urban background and rural sites in the UK atmosphere, Atmos. Environ., 44, 841–851, doi:10.1016/j.atmosenv.2009.11.026, 2010.

Yin, J., Cumberland, S. A., Harrison, R. M., Allan, J., Young, D. E., Williams, P. I., and Coe, H.: Receptor modelling of fine particles in southern England using CMB including comparison with AMS-PMF factors, Atmos. Chem. Phys., 15, 2139–2158, doi:10.5194/acp-15-2139-2015, 2015.

Young, D. E., Allan, J. D., Williams, P. I., Green, D. C., Flynn, M. J., Harrison, R. M., Yin, J., Gallagher, M. W., and Coe, H.: Investigating the annual behaviour of submicron secondary inorganic and organic aerosols in London, Atmos. Chem. Phys., 15, 6351–6366, doi:10.5194/acp-15-6351-2015, 2015a.

Young, D. E., Allan, J. D., Williams, P. I., Green, D. C., Harrison, R. M., Yin, J., Flynn, M. J., Gallagher, M. W., and Coe, H.: Investigating a two-component model of solid fuel organic aerosol in London: processes, PM1 contributions, and seasonality, Atmos. Chem. Phys., 15, 2429–2443, doi:10.5194/acp-15-2429-2015, 2015b.

Zhang, Q., Jimenez, J. L., Canagaratna, M. R., Allan, J. D., Coe, H., Ulbrich, I., Alfarra, M. R., Takami, A., Middlebrook, A. M., Sun, Y. L., Dzepina, K., Dunlea, E., Docherty, K., DeCarlo, P. F., Salcedo, D., Onasch, T., Jayne, J. T., Miyoshi, T., Shimono, A., Hatakeyama, S., Takegawa, N., Kondo, Y., Schneider, J., Drewnick, F., Borrmann, S., Weimer, S., Demerjian, K., Williams, P., Bower, K., Bahreini, R., Cottrell, L., Griffin, R. J., Rautiainen, J., Sun, J. Y., Zhang, Y. M., and Worsnop, D. R.: Ubiquity and dominance of oxygenated species in organic aerosols in anthropogenically-influenced Northern Hemisphere midlatitudes, Geophys. Res. Lett., 34, L13801, doi:10.1029/2007gl029979, 2007.

Zhang, Q., Jimenez, J. L., Canagaratna, M. R., Ulbrich, I. M., Ng, N. L., Worsnop, D. R., and Sun, Y. L.: Understanding atmospheric organic aerosols via factor analysis of aerosol mass spectrometry: a review, Anal. Bioanal. Chem., 401, 3045–3067, doi:10.1007/s00216-011-5355-y, 2011.

Zhao, R., Lee, A. K. Y., Huang, L., Li, X., Yang, F., and Abbatt, J. P. D.: Photochemical processing of aqueous atmospheric brown carbon, Atmos. Chem. Phys., 15, 6087–6100, doi:10.5194/acp-15-6087-2015, 2015.